Quaternary Science Reviews 271 (2021) 107190

Contents lists available at ScienceDirect

Quaternary Science Reviews

journal homepage: www.elsevier.com/locate/quascirev

Southern Ocean sea surface temperature synthesis: Part 2. Penultimate glacial and last interglacial

David Chandler*, Petra Langebroek

NORCE Norwegian Research Centre, Bjerknes Centre for Climate Research, Bergen, Norway

ARTICLE INFO

Article history:
Received 1 June 2021
Received in revised form
9 September 2021
Accepted 12 September 2021
Available online xxx

Handling Editor: I Hendy

Keywords:
Southern ocean
Sea surface temperature (SST)
Proxy
Quaternary
Paleoclimate
Glacial
Interglacial

ABSTRACT

The last interglacial (LIG: ~130 to 115 thousand years before present) is often used as an analogue for near-future climate warming. Antarctic Ice Sheet response to LIG warming is of particular interest, because of its implications for sea level rise. Comparison between LIG climate simulations and proxy-based reconstructions of Southern Ocean sea surface temperature (SST) remains challenging, due to high uncertainties in both reconstructions and simulations. In this two-part study, the accompanying paper (Part 1) addressed uncertainties in the SST reconstructions by evaluating proxies relevant to Southern Ocean SST, and made recommendations for which proxies and respective calibrations are most reliable on glacial-interglacial time scales in this region. In the second part (this paper), we now apply these recommendations to a synthesis of Southern Ocean SST over the penultimate glacial and LIG. Similar to previous studies, we find that LIG warming at 40°S to 60°S reached 1.6 ± 1.1 °C (annual mean) or 1.9 ± 1.3 °C (austral summer: JFM) relative to present. Annual/summer cooling in the penultimate glacial maximum reached −3.6 ± 1.0 °C/−4.0 ± 1.2 °C, similar to the last glacial maximum. Compared with the previous LIG SST syntheses, our reported uncertainties more strongly reflect geographic variability and dating errors, as we have reduced errors in the individual temperature reconstructions and do not date records by aligning peaks in their SST. However, the reconstruction errors are still important, and we do not recommend detailed interpretation of temperature records from small numbers of sites. Instead, comparisons of our new synthesis with model simulations should focus only on the regional average.

1. Introduction

Interest in the last interglacial (LIG, 130 to 115 ka before present) is motivated by its potential as an analogue for near-future climate warming, in particular the contributions of ice sheets to sea-level rise (e.g., Dutton et al., 2015; Yin and Berger, 2015; Sutter et al., 2016; Gilford et al., 2020; Turney et al., 2020a; DeConto et al., 2021). In the Southern Hemisphere, ice core evidence shows that the East Antarctic Ice Sheet (EAIS) persisted through the LIG and several previous interglacials (Petit et al., 1999; Watanabe et al., 2003; Jouzel et al., 2007), during which times global and Antarctic climates have sometimes been warmer than present (Past Interglacials Working Group of PAGES, 2016). In contrast, persistence of the West Antarctic Ice Sheet (WAIS) through interglacials is more uncertain (Mercer, 1978; Scherer et al., 1998; Vaughan, 2008; Turney et al., 2020a). During the LIG, southern mid-latitude sea surface temperatures (SSTs) and Antarctic surface air temperatures were likely less than ~2 °C and ~4 °C above present, respectively, while sea level likely reached 6–9 m above present (Kopp et al., 2009; Masson-Delmotte et al., 2011; Capron et al., 2014; Dutton et al., 2015; Hoffman et al., 2017). Although individual contributions to this sea level high stand remain debated, the potential for extensive WAIS ice loss even under moderate future warming is of concern. The regional and global climatic consequences of increasing fresh water fluxes from Antarctica into the Southern Ocean provide additional motivation for considering future ice loss (Bintanja et al., 2015; Fogwill et al., 2015; Mackie et al., 2020).

Differences in greenhouse gas concentrations, and in the seasonal and spatial distribution of insolation, between the LIG and present lead to spatial and seasonal differences in the nature of the climatic forcing; these have been discussed in detail already (Langebroek and Nisancioglu, 2014; Yin and Berger, 2015; Past Interglacials Working Group of PAGES, 2016). In the Southern

* Corresponding author.
E-mail address: dcha@norceresearch.no (D. Chandler).

https://doi.org/10.1016/j.quascirev.2021.107190

Hemisphere, thermal inertia of the ocean and efficient mixing by the Antarctic Circumpolar Current (ACC) may act to dampen regional and seasonal contrasts, in comparison to the Northern Hemisphere where the ocean basins are relatively isolated and there is much greater land cover. However, Antarctica and the Southern Ocean were likely to have been closely coupled with events in the Northern Hemisphere via the Atlantic meridional overturning circulation over millennial time scales (e.g., Holden et al., 2010; Pedro et al., 2018). The interest and complexity in Southern Ocean climate during the LIG demands high-quality paleoclimate reconstructions, and existing SST syntheses covering this region already provide valuable references in that respect (e.g., Capron et al., 2014; Hoffman et al., 2017; Turney et al., 2020b: see Table S1.1). This study builds on their efforts in two key respects.

Firstly (Part 1: Chandler and Langebroek, 2021), we focused on the several challenges associated with reconstructing SST in the Southern Ocean. Existing syntheses have mostly used temperatures as originally published, but the choices of proxies and respective calibrations are not necessarily optimal for this region. Using recent databases of modern ocean sediment samples (Tierney and Tingley, 2014, 2018; Haddam et al., 2016; Saenger and Evans, 2019; Tierney et al., 2019), and by considering problems associated with seasonality, advection, and non-thermal influences, we then made recommendations for which proxies and calibrations are considered to be most reliable for the Southern Ocean at glacial-interglacial time scales.

Secondly (in this paper) we apply these recommendations to establish a much longer LIG Southern Ocean SST synthesis than in previous studies, now including all of the penultimate glacial (MIS 6, 191 to 130 ka before present). As well as addressing interest in the penultimate glacial itself (Rohling et al., 2017; Menviel et al., 2019), this longer reconstruction should benefit LIG climate and/or ice sheet simulations for which the penultimate glacial contributes to the initialisation period (e.g., Goelzer et al., 2016; Albrecht et al., 2020). We also continue our synthesis from the LIG to the present but without adding the additional records that do not cover the LIG. This is not intended for use directly as a reconstruction - there are more detailed syntheses for the LGM and Holocene which benefit from the more numerous and higher-resolution records available for these periods (Waelbroeck et al., 2009; Gersonde et al., 2003; Barrows and Juggins, 2005; Hernández et al., 2020). Instead, it helps empricial evaluation of reconstruction errors by (i) providing a reconstructed SST anomaly at 0 ka (which should be zero) and (ii) providing 2 full glacial cycles with which to compare SST reconstructions at sites where multiple proxies are available in the same sediment core. Finally, we compare Southern Ocean SST and Antarctic surface air temperatures over the last two glacial cycles, and suggest that parameterisations employed in climatic forcings for the present interglacial in the Southern mid-to high latitudes should be robust throughout the penultimate glacial cycle, at least at the coarse (2 kyr) resolution employed here.

2. Study region and methods

The study region, informally referred to here as the Southern Ocean, is the ocean south of 40°S. This northern limit minimises inter-basin variability by restricting our study area predominantly to a region that is rapidly mixed by the Antarctic Circumpolar Current (ACC). The southern boundary in theory is the Antarctic continent, but in practice was 57°S due to a lack of records from further south. The chosen region contains few continental margins, where transport in boundary currents can cause problems for proxy reconstructions (see Part 1). Modern Southern Ocean dynamics in the context of global climate are described elsewhere (e.g., Rintoul, 2018).

The available SST proxies fall into two broad groups: geochemical and assemblage. The former uses an empirical calibration, and the latter a statistical approach using transfer functions or the modern analogue technique (MAT). Our detailed evaluation in Part 1 recommended two geochemical proxies (C_{37} alkenones and *Globigerina bulloides* Mg/Ca ratio) and two assemblage-based proxies (foraminifera and diatoms). Fortuitously, this selection includes one heterotrophic group and one phototropic group in each of the two proxy groups. This diversity minimises the poorly-constrained influences of past changes in seasonality, habitat depth, or other factors that might affect one group more than another.

Data for most SST reconstructions were obtained from the Pangaea (https://www.pangaea.de) or NOAA (https://www.ncdc.noaa.gov/data-access/paleoclimatology-data) archives. Otherwise, data were requested from the authors, or digitised from the original publication (using WebPlotDigitizer: https://apps.automeris.io/wpd/). Digitizing was only needed at 3 sites (Table A1) and was the least favoured option because it is less accurate and it is not possible to clearly identify individual data points in line plots.

Anomalies are reported relative to the World Ocean Atlas (WOA2018: Locarnini et al., 2018). Modern SST at each site was bilinearly interpolated from the four closest WOA18 grid points. Capron et al. (2014) found the choice of modern ocean atlas introduced little error (±0.2 °C), far smaller than the errors in the reconstructions. The reconstructed core-top temperatures are not used as the reference, because not all sites have a core-top sample. Instead the available core tops were used to assess errors for the subset of records that does have a core-top sample, since the modern sediments should (in theory) yield a modern SST anomaly of zero.

Following recommendations in Part 1, we focus only on the Southern Ocean mean SST anomaly, and do not analyse records from individual sites or sub-regions.

2.1. Selection criteria

To reduce the uncertainty in our mean regional SST anomaly, we can reduce the error in individual reconstructions and/or increase the number of reconstructions, considering that uncertainty in the mean of n independent samples increases as $\sigma/\sqrt{n}$. Increasing n requires the selection of lower-quality records that could increase σ, but also samples a greater area of the Southern Ocean, so that our regional mean is more representative. Inclusivity is ultimately a subjective compromise between quality and quantity. Suitability of each proxy was evaluated by reviewing their individual strengths and weaknesses (Part 1). Previous syntheses (Capron et al., 2014; Hoffman et al., 2017; Turney et al., 2020b) have not been selective in this respect, although Hoffman et al. (2017) recalculated the contributing alkenone and Mg/Ca records using consistent calibrations. However, not all of the many available calibrations are optimal for the Southern Ocean. This motivated our use of consistent calibrations in this study, following the evaluation in Part 1.

2.2. Temperature calibrations

Temperatures based on diatom assemblages were used as originally published. Temperatures for the other proxies were calculated following the recommendations in Part 1, summarised briefly as follows.

For the alkenone $U^{K'}_{37}$ index we used the Prahl et al. (1988) annual SST calibration, and a revised summer SST calibration (Part 1) based on a core-top sediment database (Tierney and Tingley, 2018). The latter lies between the Sikes and Volkman (1993) and

Müller et al. (1998) calibrations. Annual and summer temperatures in °C are:

$$\text{Annual SST} = 30.3U^{K'}_{37} - 1.30$$
$$\text{Summer SST} = 29.7U^{K'}_{37} + 0.90$$

The respective RMSEPs are 1.6 and 1.7 °C. The advantages and disadvantages of using a single index to reconstruct both annual and summer SST were discussed in Part 1, but most importantly we note that the implicitly fixed seasonality prevents comparison of summer and annual temperature reconstructions.

For *G. bulloides* Mg/Ca we used a revised calibration from Part 1, based on core-top sediment databases (Saenger and Evans, 2019; Tierney et al., 2019). Again, temperatures are in °C:

$$\text{Annual SST} = 13.0\ln(1.23\text{Mg/Ca})$$

The RMSEP is 2.6 °C.

For the foraminifera assemblages we calculated annual and summer SST using the modern analogue technique and core-top sediment census counts in the Haddam et al. (2016) database. We used the unweighted mean of the 7 best analogues, based on thirteen selected taxa (see Part 1), yielding respective annual and summer RMSEPs of 1.2 and 1.4 °C.

2.3. Age models and chronology

The LIG and penultimate glacial are well beyond the ~40 ka range of radiocarbon dating. Instead, dating of the Southern Ocean sediment cores can be achieved by aligning one or more proxy records in the sediment core with a suitable target, such as a global or regional benthic foraminiferal δ^{18}O stack (Lisiecki and Raymo, 2005; Lisiecki and Stern, 2016), a proxy record in another marine sediment core (e.g., Xiao et al., 2016; Hoffman et al., 2017), or an ice core proxy record (Capron et al., 2014; Hoffman et al., 2017). Each method has distinct strengths and weaknesses.

Since we are reconstructing SST, the simplest and most convenient approach is to align the reconstructed SST with another temperature. In their LIG SST syntheses, Capron et al. (2014) and Hoffman et al. (2017) assumed that SST across all three main basins of the Southern Ocean evolved synchronously with Antarctic ice sheet air temperature at millennial time scales. On this basis, Capron et al. (2014) aligned all their Southern Ocean SST reconstructions directly with the high-resolution EPICA Dome C (EDC) air temperature reconstruction (Jouzel et al., 2007). This method was preferred over alignment of benthic foraminiferal calcite oxygen isotopes (δ^{18}O), because of potentially asynchronous changes in benthic δ^{18}O between ocean basins during glacial terminations (Lisiecki and Raymo, 2009). In a combined approach, Hoffman et al. (2017) aligned the SST of one high-resolution 'reference core' in each Southern Ocean basin with EDC air temperature, but then aligned the remaining cores in each basin with the respective basin's reference core using benthic δ^{18}O. This allowed for some intra-basin variability in the timing of SST peaks. Using SST for dating has the advantage of being applicable to all available cores, some of which do not have δ^{18}O. However, three important disadvantages are: (1) this method artificially amplifies the reconstructed peak interglacial warming (and glacial cooling) if local SST changes are not synchronous across the region; (2) the SST reconstructions themselves often have poor signal-to-noise ratios (see Part 1 and Section 3.2), and (3), age models suffer from ambiguity if SST peaks based on different proxies or seasons at the same site are separated by several thousand years (e.g., site FR1/94-GC3: Pelejero et al., 2006; De Deckker et al., 2019).

Dating records by aligning benthic δ^{18}O with a global or regional stack (Imbrie et al., 1984; Lisiecki and Raymo, 2005; Lisiecki and Stern, 2016) has the advantage that the SST reconstructions and age models are independent. However, foraminiferal δ^{18}O depends on both seawater $\delta^{18}O_w$ (driven largely by global ice volume at millennial time scales) and on temperature, according to the paleotemperature equation (Eq. S2.1) (Urey et al., 1951; Shackleton, 1974). Neither $\delta^{18}O_w$ nor bottom water temperature changes were necessarily globally synchronous, potentially introducing dating errors of 2–3 kyr (Lisiecki and Stern, 2016). Another problem is that many records only have planktic δ^{18}O (or no δ^{18}O data at all). Several SST reconstructions in the Southern Ocean have used planktic δ^{18}O for age modelling, but because planktic δ^{18}O likely includes an important SST signal, we could then return to *some* of the drawbacks just described for dating by SST.

Turney et al. (2020b) partly circumvented the problem of dating in their global LIG SST synthesis by reporting temporal averages for 129 to 116 ka and for the late-glacial (140–135 ka), rather than constructing a time series. However, their method does still need some age control to identify the LIG and penultimate glacial maximum (PGM), and the ~13 kyr time scale of the LIG-average SST is likely too long to capture climatic changes important for ice sheet or climate simulations over that period.

In Section S2 we discuss the use of foraminiferal δ^{18}O in more detail, and estimate the relative contributions of temperature changes and seawater $\delta^{18}O_w$ changes to foraminiferal calcite δ^{18}O over glacial-interglacial time scales in the Southern Ocean. On that basis, we choose to date records using benthic δ^{18}O where possible, planktic δ^{18}O as an alternative, and exclude other records (e.g. those aligned directly by SST). This was justified as follows.

1. SST reconstructions use different organisms from six planktic groups, and are susceptible to important non-thermal influences (see Part 1). The resulting age models would suffer from these same problems. In contrast, age models based on SST-dependent planktic δ^{18}O are more consistent, as they are still partly driven by seawater $\delta^{18}O_w$ and involve a much lower diversity of organisms (only two species – *G. bulloides* and *N. pachyderma* – from one planktic group).
2. Habitat tracking, which may dampen the SST signal in geochemical SST proxies (see Part 1), is a hindrance to SST reconstructions but is helpful when using planktic δ^{18}O for dating because the water temperature signal in δ^{18}O is dampened relative to the water isotopic $\delta^{18}O_w$ signal.
3. Advection of planktic organisms may introduce a large error in SST reconstructions for some proxies, because organisms in the sediments could have travelled many hundreds of kilometres from their surface habitat (see Popova, 1986; van Sebille et al., 2015; Nooteboom et al., 2019, and the discussion in Part 1). This could clearly degrade age models based only on SST. However, *G. bulloides* and *N. pachyderma* are both relatively fast sinkers, and their fossils should have a relatively local origin in comparison to other planktic groups (Fig. 1 in Part 1).

Our decision is a preferred but certainly not perfect solution. Even when using only foraminiferal δ^{18}O for age models, further challenges arise because of varying resolutions (between and within records), and because in practice the picking of age tie points is subjective. The challenge of consistently identifying tie points is evident in Fig. S2.2.

The final question here is what chronology the records should be transferred onto, since the several chronologies used in the original temperature reconstructions differ by a few thousand years during the penultimate glacial cycle (Imbrie et al., 1984; Martinson et al., 1987; Lisiecki and Raymo, 2005; Parrenin et al., 2007; Bazin et al., 2013; Veres et al., 2013; Lisiecki and Stern, 2016). Since we

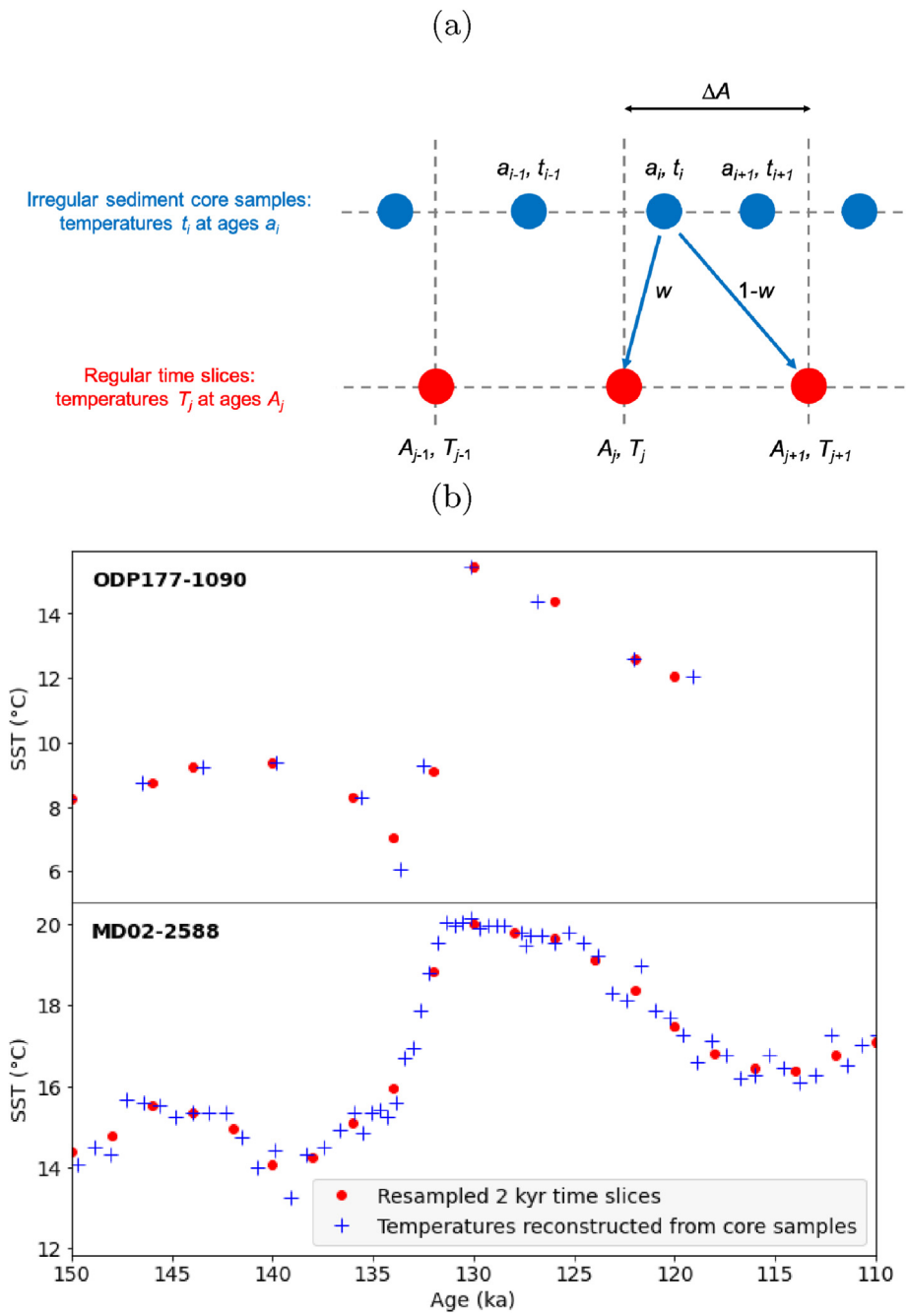

Fig. 1. Resampling of irregular temperature records onto regular time slices. (a) Temperature sample t_i at age $_i$ contributes to the temperatures T_j, T_{j+1} at neighbouring time slices A_j, A_{j+1}, with weightings of w and $1 - w$. See Section 2.5 for details. (b) Example temperature records (blue) resampled to 2 kyr resolution (red). For the high-resolution record reconstructed from alkenones at MD02-2588 (Govin et al., 2009), each time slice is based on several samples. In the low-resolution alkenones record from PS3489-2/ODP177-1090 (Martínez-Garcia et al., 2009), each time slice is based only on one sample, and some time slices are missing. (For interpretation of the references to colour in this figure legend, the reader is referred to the Web version of this article.)

are selecting records with foraminiferal $\delta^{18}O$, and for consistency with many of the original publications, a convenient chronology is LR04 (Lisiecki and Raymo, 2005). Using leads/lags between LR04 and the other chronologies (Imbrie et al., 1984; Martinson et al., 1987; Lisiecki and Raymo, 2005; Parrenin et al., 2007; Bazin et al., 2013; Veres et al., 2013), we can then transfer all selected records onto LR04 without establishing new age models. Age modelling is inevitably a subjective task, and using the authors' original age models thus retains uncertainties reflecting 'expert opinion' in this aspect of the synthesis. Such uncertainties are evident when comparing the age models established by Capron et al. (2014) and Hoffman et al. (2017) for the same sites: even using their quite similar approaches, their respective ages were almost identical at some sites but differed by 5–10 kyr at others (e.g., sites PS2489-2 and ODP177-1089).

A significant disadvantage of transferring the original age models to LR04 is the possibility of asynchronous changes in benthic $\delta^{18}O$ between the main Southern Ocean basins (Lisiecki and Raymo, 2009; Capron et al., 2014; Lisiecki and Stern, 2016). This is illustrated in the recent LS16 chronology (Lisiecki and Stern, 2016)

(plotted for the LIG in Fig. S2.1), where the end of the penultimate glacial $\delta^{18}O$ maximum and start of the LIG $\delta^{18}O$ minimum differ by up to 3 kyr between ocean basins. To take advantage of this more recent LS16 chronology, which is based on many more sites in the Southern Ocean than the older LR04 (Lisiecki and Raymo, 2005; Lisiecki and Stern, 2016), we revise age models for our selected sites where possible by aligning their benthic $\delta^{18}O$ with the respective basin's LS16 benthic stack. For planktic $\delta^{18}O$, we assume that isotopic changes were synchronous across all Southern Ocean basins (due to rapid mixing by the ACC) and thus align records with the mean across the four relevant LS16 regional water masses (deep South Atlantic, deep Indian, deep Pacific and Intermediate Pacific: see Lisiecki and Stern, 2016), recognising the potenial errors as noted in Section S2.

2.4. Correction for advection

Correcting reconstructed SSTs for lateral advection of their planktic hosts was considered important in the most recent SST synthesis (Turney et al., 2020b). However, in Part 1 we highlighted four important reasons to not use a drift correction in the Southern Ocean. Briefly, these are: (1) the sinking rate and varies widely between different proxies, and is poorly constrained, so assuming the same sinking rate across all proxies is not appropriate; (2) drift corrections were not applied to empirical calibrations or to training data based on core-top sediments, so are not appropriate in reconstructions using these uncorrected calibrations; (3) the drift correction may be sensitive to changes in ocean circulation, which has likely varied under past climates; and (4) 'advection' used here in the loose sense also includes a diffusion component (related to the eddy diffusivity of the ocean), which is a random process that cannot necessarily be reversed in back-trajectory modelling (e.g., Batchelder, 2006). Instead we have chosen to exclude proxies considered in Part 1 to be susceptible to strong advection bias.

2.5. Re-sampling and stacking records

The published sediment core records have inconsistent resolutions and time periods. Before the records can be combined (stacked) into a regular time series, they need re-sampling to a common resolution. Specifically, each original record of n temperatures t_i at ages a_i ($i = 1 \ldots n$) needs re-sampling to a common resolution (Δa), at time slices $A_j = j\Delta a$ ($j = 0 \ldots J$) (Fig. 1). Here, to cover the period from 200 ka to present at 2 kyr resolution, we use $\Delta a = 2$ kyr and $J = 100$. Simple linear interpolation of high-resolution records onto a low resolution time series could result in many samples not contributing to the re-sampled time series. Meanwhile, linear interpolation of low-resolution records onto a higher resolution time series can assign temperatures to times far from the nearest sample; in this case, linear (or any other) interpolation is not appropriate without some additional constraint. Instead, the temperature T_j at each time slice A_j is calculated as a linearly weighted average of all samples within a time range $A_j \pm \Delta a$. Thus, for each record we calculate temperatures T_j at time slices A_j as follows (see also Fig. 1).

Under this scheme, time slices j further than $\Delta a/2$ from any data point in the core record will remain flagged as False and will not be assigned a temperature from that record. High-resolution records will have a temperature assigned to most time slices, sometimes calculated from several samples. Low-resolution records will only have temperatures assigned to intermittent time slices, and those time slices are likely to be based only on one sample. Examples of both cases are shown in Fig. 1. For sites with low resolution and low sedimentation rates (e.g., 2 cm/kyr at CHAT-1K, E49−19 and R657: Weaver et al., 1998; Rickaby and Elderfield, 1999), we also note that a single sample could span more than 2 kyr. For our purposes the date of the sample is taken as that corresponding to the reported sample depth. The most likely consequence of including a minority of low-resolution records is some slight temporal smoothing of regional mean temperature changes. The regional mean SST anomaly at each time slice is the mean across all sites contributing records to that time slice.

Start with sums $S_{T,j} = 0$, $S_{W,j} = 0$, and flag F_j = False for all time slices j.
For all samples $i = 1 \ldots n$:
  Find j such that sample age a_i lies between time slices A_j and A_{j+1}.
  Linear weighting $w = (a_i - A_j)/\Delta a$.
  Add wt_i to $S_{T,j}$; add $(1 - w)t_i$ to $S_{T,j+1}$.
  Add w to $S_{W,j}$; add $(1 - w)$ to $S_{W,j+1}$.
  If $w < 0.5$, set F_j = True.
  If $w \geq 0.5$, set F_{j+1} = True.
For each time slice $j = 0 \ldots J$:
  If Fj = True then:
    assign temperature $T_j = S_{T,j}/S_{W,j}$
  else:
    assign no temperature for T_j.
All valid time slices have now been assigned a temperature.

2.6. Uncertainties

When comparing this or past syntheses with climate simulations, it is important to consider what exactly the reported uncertainty represents.

One approach to estimating uncertainties in the regional SST anomaly is to separately estimate dating errors, analytical errors, and calibration errors at each site. These are then propagated through each step of the synthesis in a Monte Carlo simulation (e.g., Capron et al., 2014; Hoffman et al., 2017). This has the advantage that each individual site is assigned an error, but has some important disadvantages for our application. First, spatial variance is not included. If a hypothetical reconstruction technique were to be developed with negligible dating and calibration error, the Monte-Carlo simulation would return a negligible uncertainty in regional mean SST for the Southern Ocean - even if records are sparsely scattered across a large area. This is because the reported error is in *the mean SST at the chosen sites*, not *across the whole region*. In addition, many sources of uncertainty (e.g., from seasonality, particle drift and non-thermal influences: see Part 1) are not well quantified even under modern conditions, so their uncertainty will be even more poorly constrained under past climates.

In a synthesis of records, an alternative is to use a confidence interval based simply on the mean and standard deviation across all

the records. Here, each anomaly is treated as a random sample from the distribution of Southern Ocean SST anomalies. This will empirically include geographical variability and most methodological errors, but it will exclude bias in calibrations of geochemical proxies. For example, the linear Prahl and Wakeham (1987) calibration is used to convert alkenone $U^{K'}_{37}$ index to SST, and the same calibration parameters are used to reconstruct all records based on alkenones, so errors in the calibration parameters will not be fully accounted for in the final mean SST confidence interval. This could be an important disadvantage where all records use the same proxy, but becomes less important as the number of included proxy types increases.

We are using four proxies selected from both main classes (assemblage and geochemical). Therefore, we use the mean and confidence interval of the stacked records as a simple but effective estimate of uncertainty that includes spatial variance and random reconstruction errors. We can further empirically evaluate errors using the reconstructed SST at 0 ka (which should have an anomaly of zero), and by comparison of two reconstructions from the same sediment core.

3. Results

3.1. Penultimate glacial and last interglacial SST

Reconstructed SST anomalies at 2 kyr resolution show the expected glacial-interglacial cycles, reaching LIG maxima of +1.6 ± 1.1 °C (annual) and +1.9 ± 1.3 °C (summer), in both cases at 126 ka (Figs. 2 and 3). Using linear interpolation to estimate zero-crossing points, the positive temperature anomaly most likely lasted from 131 to 119 ka (annual) or 132 to 118 ka (summer). There is considerable uncertainty in this duration as the 95% confidence intervals for the mean anomalies include zero for several thousand years either side of the LIG optimum.

Cooling in the penultimate glacial reached −3.6 ± 1.0 °C (annual) and −4.0 ± 1.2 °C (summer), but in contrast to the LIG, there was no well-defined peak anomaly. Instead the long-term temperature trend was relatively flat, with multiple minima of similar magnitude between 186 and 142 ka (Fig. 2. However, the uncertainties are relatively wide through the PGM, due to the lower number of records rather than a wider spread, and we cannot be sure whether these minima (or even the overall flat trend) reflect real events or reconstruction errors.

3.2. Sensitivity and errors

3.2.1. Sensitivity to resolution

Sensitivity of the reconstruction to the chosen resolution was tested by repeating the method at coarser resolution (4 kyr: Table 1). Comparing 2 kyr and 4 kyr, we find that differences in the strengths of the LIG optimum and PGM are within the uncertainties. Therefore, our reconstructed temperatures show only weak sensitivity to our choice of 2 kyr resolution. Finer resolution (e.g., 1 kyr) is of course also possible, but is not meaningful in our study given the dating errors, and at 1 kyr resolution there would be many time slices with few contributing sites. Nevertheless, a few high-resolution sites in the Indian and Pacific ocean basins can provide further insights into localised sub-millennial scale variability, as discussed in their original publications. These include MD02-2488 (Govin et al., 2009), MD02-2588 (Romero et al., 2015), MD88-770 (Barrows et al., 2007), MD97-2120 & MD97-2121 (Pahnke et al., 2003; Pahnke and Sachs, 2006), and SO136-GC3 (Pelejero et al., 2006; Barrows et al., 2007).

3.2.2. Sensitivity to choice of proxies

Annual SST was reconstructed with C_{37} alkenones, foraminifera assemblages and *G. bulloides* Mg/Ca, while summer SST was reconstructed with C_{37} alkenones, foraminifera assemblages and diatoms assemblages. In our evaluation of these proxies (Part 1), the alkenones and foraminifera assemblages were considered as the most reliable. Hence, we can repeat the synthesis using only alkenones and foraminifera assemblages. Conveniently, this also provides us with annual and summer SST time series based on the same two proxies and almost the same sites (just 2 foraminifera sites have only annual SST). Results based only on these two proxies are very similar to those with three proxies (Table 1). Importantly, the standard deviation of annual or summer SST at the LIG peak (126 ka) increased, by 0.2 °C or 0.3 °C, after excluding Mg/Ca or diatoms, respectively. This suggests that both Mg/Ca- and diatom-based SSTs are consistent with the alkenone- and foraminifera assemblage-based SSTs (otherwise, the standard deviation would have been smaller after their exclusion). Therefore, inclusion of *G. bulloides* Mg/Ca and diatoms should help to reduce overall uncertainty in the regional mean SST anomaly.

3.2.3. Choice of revised calibrations

Comparison of SST time series based on individual proxies is useful but has limited scope due to the low number of contributing sites in many time slices (particularly prior to the LIG). However, there are sufficient sites to compare the foraminifera assemblage SST reconstruction with the combined geochemical reconstructions (alkenones and *G. bulloides* Mg/Ca). This is an interesting comparison between the faunal and geochemical proxy groups, and is possible using the originally published records as well as using our revised/recommended calibrations. The comparison is helped by the similar spatial distributions of sites for the two proxy groups (Fig. 4b). To test for significant differences between the means of the two proxy groups at each time slice, we use Welch's *t*-test, which allows for unequal variances and sample sizes (Welch, 1947).

For the original reconstructions, we use the same selection of sites as that used in the revised synthesis (Table A2), but use the temperatures as originally published. We find the foraminifera assemblage SST is consistently, and often significantly cooler, than the geochemical group.

With our recommended calibrations in Section 2.2, the two time series for annual mean SST are very consistent through both glacial cycles (Fig. 4a). We find few significant differences, although this is partly due to high variance and low *N* for many time slices (particularly in MIS 6). There is an indication that the foraminifera assemblage SST is a little cooler through the interglacials, but that difference is not significant.

Overall, comparing the original and revised reconstructions in this way provides further evidence that we have reduced the bias associated with the different proxies.

3.2.4. Temperature bias

The reconstructed SST anomalies at 0 ka, which should be zero, are +0.3 ± 1.0 °C (annual) and +0.8 ± 1.1 °C (summer). These represent a weak (not statistically significant) warm bias in the reconstruction. The magnitude of this bias is poorly constrained because only 13 of 29 annual and 13 of 27 summer SST records have a temperature at 0 ka. However, the bias is considerably smaller than the amplitudes of (1) the glacial-interglacial temperature changes and (2) the peak LIG warming relative to present. Therefore, the positive LIG regional mean SST anomaly is unlikely to simply reflect a warm bias in the temperature reconstructions.

For comparison, the annual and summer SST anomalies at the same sites in the original reconstructions were +0.6 ± 1.1 °C (annual) and +0.8 ± 3.5 °C (summer). The wide confidence interval

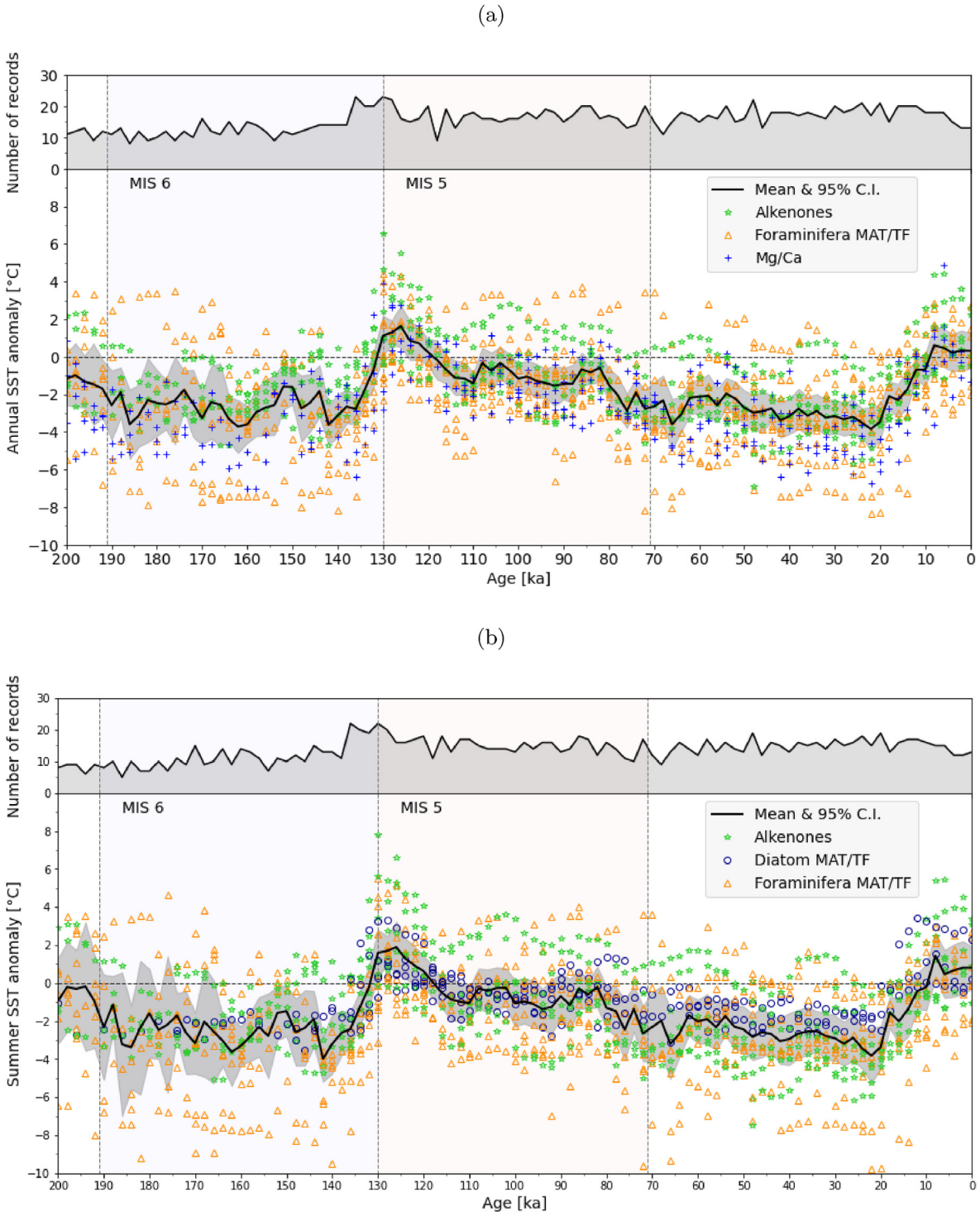

Fig. 2. Time series of revised SST anomalies at the selected sites in Table A1, for (a) annual and (b) summer (JFM). Each record has been revised following recommendations in Part 1, then resampled to 2 kyr resolution (Section 2.5 and Fig. 1). Anomalies are relative to the 2005 to 2017 SST (World Ocean Atlas, 2018: Locarnini et al., 2018). Marine isotope stage (MIS) boundaries follow Lisiecki and Raymo (2005). Records have been transferred to the Lisiecki and Stern (2016) chronology.

in the original summer SST anomaly arises due to fewer contributing records (5 original, 9 revised), because the alkenone $U^{K'}_{37}$ index was mostly used only for annual SST, whereas we have used it for summer too.

3.2.5. *Duplicate reconstructions from one core*

Comparison of duplicate SST reconstructions from a single core provides a valuable empirical estimate of errors in reconstructed SST, since errors in dating are eliminated. Here we compare the four sites which have multiple proxies with the same inferred seasonality, and use the re-sampled 2 kyr data for the period 200 to 0 ka (Fig. 5). We find a root mean square difference (RMSD) of 1.0 to 1.7 °C and a mean bias within ±0.9 °C when using the recommended calibrations (blue bars in Fig. 5). Here the mean bias is

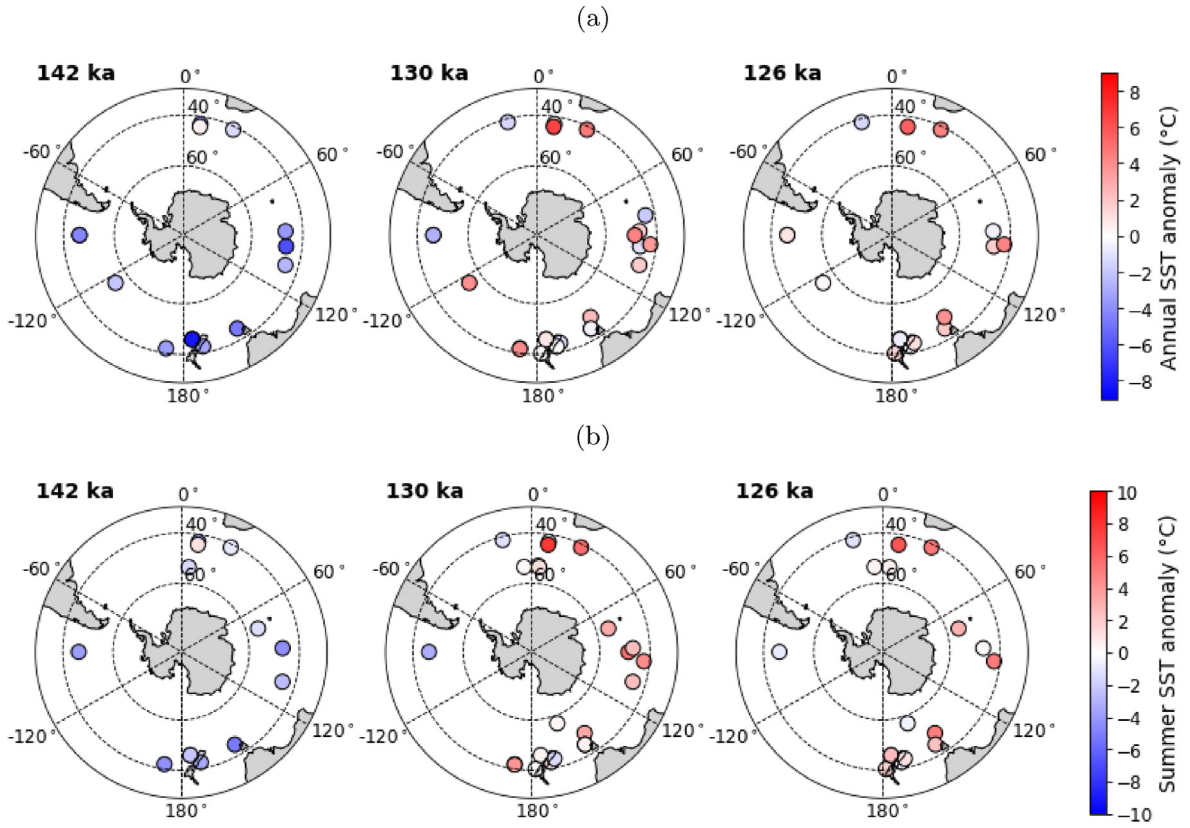

Fig. 3. (a) Annual and (b) summer SST anomalies at individual core sites, for time slices corresponding to the penultimate glacial maximum (PGM, at 142 ka), early last interglacial (LIG) (130 ka), and LIG optimum (126 ka). Each record has been revised following recommendations in Part 1, and plotted anomalies are for 2 kyr time slices (Section 2.5 and Fig. 1). Anomalies are relative to the 2005–2017 SST (World Ocean Atlas, 2018: Locarnini et al., 2018).

Table 1
Summary of Southern Ocean SST anomalies and their sensitivity to choices of synthesis method. *The penultimate glacial comprises several similar minima between 186 and 142 ka. Figures quoted here are for 142 ka **The synthesis on the LR04 chronology uses the original age models, transferred from their chronology to LR04 where necessary.

	Annual SST anomaly	Summer (JFM) SST anomaly
Total number of records, of which:	29	27
Alkenones	9	9
Diatom assemblage	–	5
Foraminifera assemblage	15	13
G. bulloides Mg/Ca	5	–
Reconstructed SST at 0 ka (represents bias)	+0.3 ± 1.0 °C	+0.8 ± 1.1 °C
LGM minimum	−3.9 ± 1.1 °C (24 ka)	−3.8 ± 1.5 °C (22 ka)
LIG maximum	**+1.6 ± 1.1°C (126 ka)**	**+1.9 ± 1.3°C (126 ka)**
PGM	**−3.6 ± 1.0°C (*)**	**−4.0 ± 1.2°C (142 ka)**
Duration of positive anomaly	131 to 119 ka	132 to 118 ka
Mean latitude of sites	44.2°S	45.6°S
Latitude range	40.4 to 54.2°S	40.4 to 56.7°S
Sensitivity to resolution		
LIG maximum, 2 kyr resolution	+1.6 ± 1.1 °C (126 ka)	+1.9 ± 1.3 °C (126 ka)
LIG maximum, 4 kyr resolution	+1.3 ± 0.7 °C (128 ka)	+1.7 ± 0.9 °C (128 ka)
PGM, 2 kyr resolution	−3.6 ± 1.0 °C (*)	−4.0 ± 1.2 °C (*)
PGM, 4 kyr resolution	−3.5 ± 1.3 °C) (*)	−3.3 ± 0.8 °C) (*)
Sensitivity to chosen proxies	*No Mg/Ca*	*No diatoms*
LIG maximum	+1.7 ± 1.4 °C (126 ka)	+2.0 ± 1.7 °C (126 ka)
PGM	−3.8 ± 1.2 °C (*)	−4.2 ± 1.2 °C (142 ka)
*Sensitivity to dating***		
LIG maximum: LR04	+1.5 ± 0.9 °C (124 ka)	+1.9 ± 1.1 °C (124 ka)
PGM: LR04	−3.9 ± 1.2 °C (*)	−3.9 ± 1.6 °C (*)

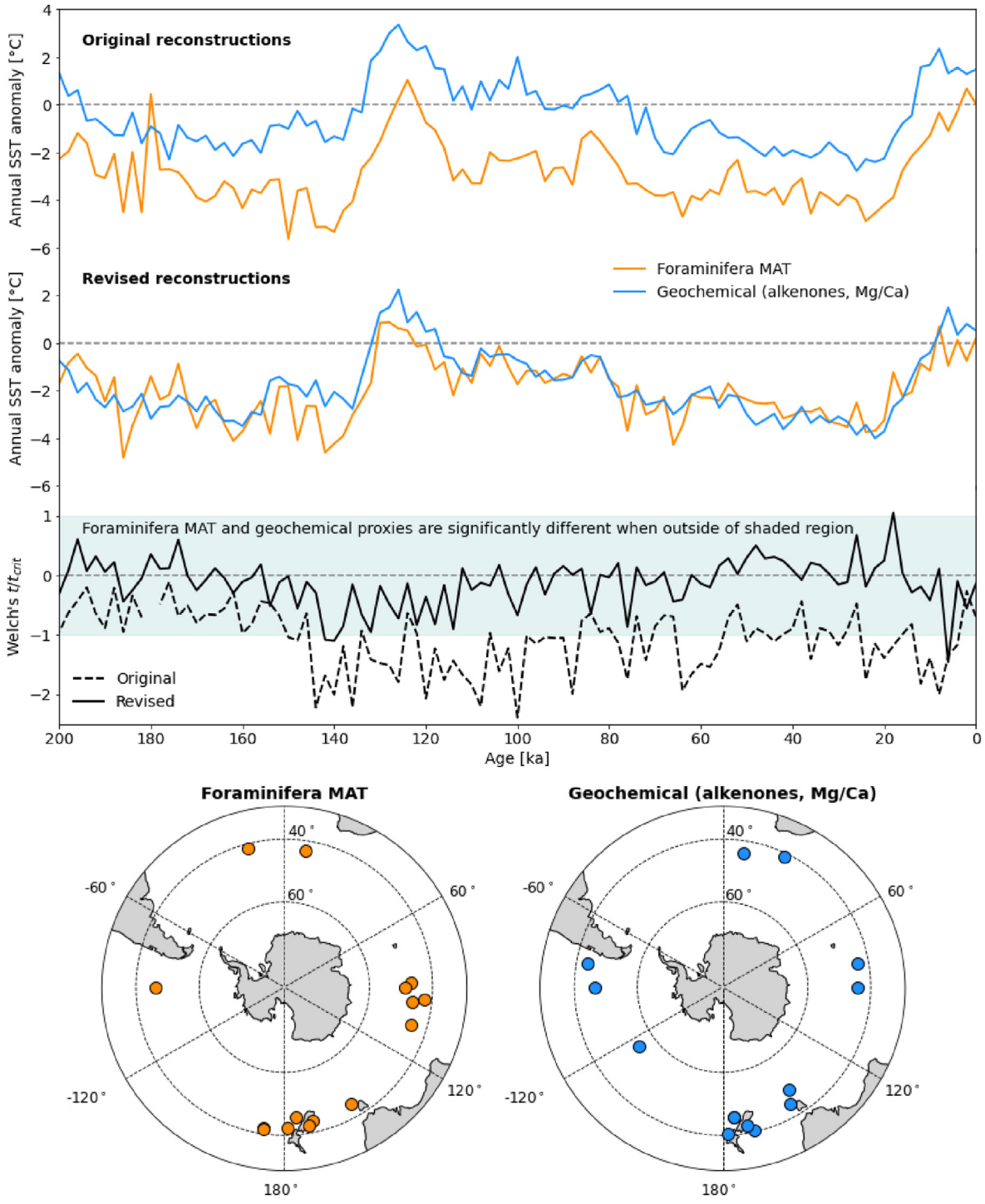

Fig. 4. Top: Original and revised annual SST reconstructions at the sites selected in the revised synthesis, but separated by proxy group (foraminifera assemblage; geochemical). Differences between the means of the two groups are quantified using Welch's *t*-test, and are significant ($p < 0.05$) *outside* of the green shading when $|t/t_{crit}| > 1$. Differences between the two proxy groups are clearly reduced in the revised synthesis, compared to those in the original publications. Bottom: locations of the contributing SST records. (For interpretation of the references to colour in this figure legend, the reader is referred to the Web version of this article.)

simply the difference in temperature between the respective records, averaged over time slices which have a temperature for both records. Too few comparisons are available with which to meaningfully assess the bias or reliability of individual proxies. Nevertheless, these results are encouraging from a number of aspects. Firstly, the RMSDs are within the estimated RMSEPs for individual proxies (Part 1), suggesting that the estimated RMSEPs provide a realistic measure of the calibration errors, despite the potential for spatial autocorrelation to artificially reduce estimated errors in core-top datasets (Guiot and de Vernal, 2011a,b; Telford and Birks, 2011). Second, the low bias (<0.9 °C) indicates that offsets between proxies are likely to be much smaller than the magnitude of glacial-interglacial cycles. This is important in a synthesis of records from different proxies, because an apparent change in regional mean SST

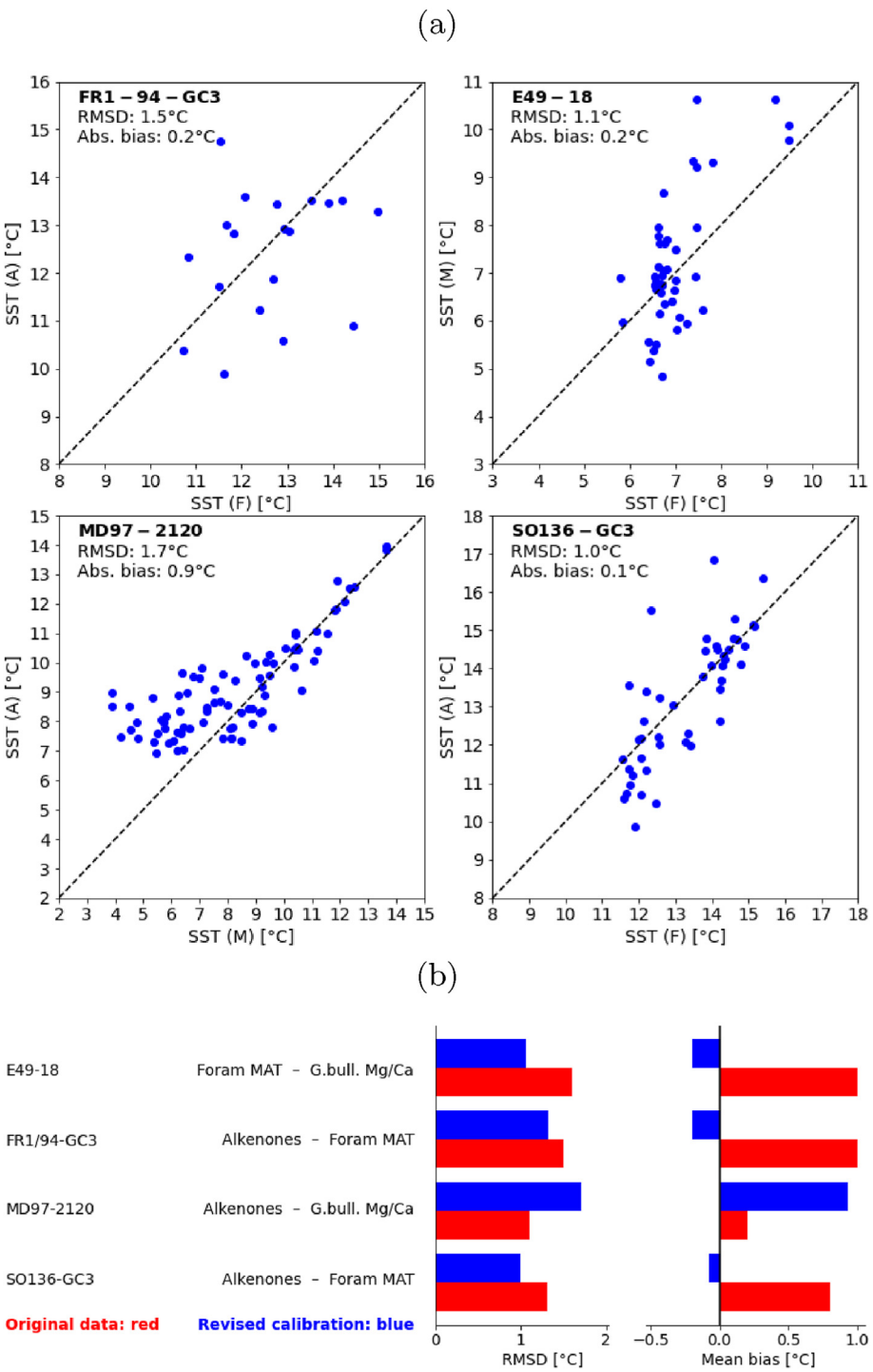

Fig. 5. Comparison of temperature reconstructions using different proxies in the same core, for the period 200 ka to present. (a) Annual SSTs reconstructed using the recommended calibrations (see Part 1) and then resampled to 2 kyr resolution as described in Section 2.5. (b) Comparison of the root mean square difference (RMSD) and bias in the records as originally published (red bars) and following revision using the recommended calibrations (blue bars). Original data sources are provided in Table A1. Proxy abbreviations are alkenones (A), foraminifera assemblage (F), and *G. bulloides* Mg/Ca (M). (For interpretation of the references to colour in this figure legend, the reader is referred to the Web version of this article.)

is less likely to simply reflect a changing contribution of the different proxy types. Thirdly, the revised SSTs show reduced RMSD and reduced bias in three out of four cases when compared to the original published SSTs. This justifies our efforts to use consistent, updated calibrations optimised for the Southern Ocean. Nevertheless, for specific time slices we find temperature differences commonly reaching 3 °C, exceptionally 5 °C, affecting both glacial climates and warm climates, again suggesting caution when analysing single records.

3.2.6. *Sensitivity to dating*

In Section 2.3 above we discussed briefly how the records

should be dated, and chose to align records to the regional benthic $\delta^{18}O$ stacks (LS16: Lisiecki and Stern, 2016) rather than transferring the published age models to the older LR04 chronology (Lisiecki and Raymo, 2005) used for many of the original reconstructions. In practice, we find this choice makes little difference to the final result (Table 1). This is probably because the errors in dating are still dominated by the resolution of the records rather than inter-basin variability in isotopic changes. Also, the 2 kyr resolution of the synthesis is relatively coarse in comparison to the time scale of inter-basin variability (<3 kyr).

3.3. Regional differences

We do not analyse in detail the differences between ocean basins, despite the potential value this could have in gaining a better understanding of what is driving the observed changes in SST. Such comparison is of questionable value because the relative contributions of each proxy type, and the mean latitude of the contributing sites, vary between ocean basins. Furthermore, the relatively small number of sites in each basin (Fig. 3) leads to uncertainties in mean anomalies that are far greater than any apparent differences. Qualitatively, we do not observe any obvious regional cold or warm clusters in the time slices for the PGM (142 ka), early LIG (130 ka) or LIG optimum (126 ka) (Fig. 3).

Although we cannot meaningfully compare different regions, we can analyse how the correlation between pairs of records varies with geographic separation. For N records, we have $N(N-1)/2$ pairwise comparisons, giving us a much larger sample size than we would have if comparing regional means. First, we calculate the distances D_{ij} between each pair of sites (i, j). D is in the circumpolar sense, rather than the shortest (great circle) distance. For respective longitudes Lon_i, Lon_j in the range -180 to $+180$°E, and latitudes Lat_i, Lat_j in the range -60 to -40°N:

$$\Delta\mathrm{Lon} = |\mathrm{Lon}_i - \mathrm{Lon}_j| \text{ if } |\mathrm{Lon}_i - \mathrm{Lon}_j| < 180, \text{ else } \Delta\mathrm{Lon} = 360 - |\mathrm{Lon}_i - \mathrm{Lon}_j|;$$

$$\Delta\mathrm{Lat} = |\mathrm{Lat}_i - \mathrm{Lat}_j|.$$

The average latitude is $\mathrm{Lat}_{\mathrm{Av}} = (\mathrm{Lat}_i + \mathrm{Lat}_j)/2$, and the radius of the Earth is R_E. Meridional and zonal displacements X and Y, respectively, are then:

$$X_{ij} = (\pi/180) R_E \Delta\mathrm{Lon} \times \cos(\mathrm{Lat}_{\mathrm{Av}}),$$

$$Y_{ij} = (\pi/180) R_E \Delta\mathrm{Lat}.$$

This a reasonable approximation for a narrow latitude band. Finally.

$$D_{ij} = (X_{ij}^2 + Y_{ij}^2)^{1/2}.$$

Now we correlate SSTs at the respective pairs of sites using Spearman's rank correlation, yielding $N(N-1)/2$ pairs of D_{ij}, ρ_{ij} with $i = 1$ to $N-1$, $j = i+1$ to N.

For both annual and summer SST, 2D histograms of (D_{ij}, ρ_{ij}) (Fig. 6a,d) show generally strong site-to-site correlations at all separations, with only a slight tendency towards an increasing number of weaker correlations (e.g., $\rho_{ij} < 0.5$) as separation increases. There are two clear clusters in the histogram for annual SST (Fig. 6a), arising partly because the sites are themselves clustered (Fig. 3). In Fig. 6a, one cluster of sites at close proximity $D_{ij} <$ 2000 km shows relatively strong site-to-site correlation ($0.4 < \rho_{ij} < 0.8$). The second cluster includes sites separated by ~7000 km and shows slightly weaker site-to-site correlation ($0.4 < \rho_{ij} < 0.7$). This second cluster of points with slightly weaker correlation comprises site pairs either in different ocean basins or widely separated in the Pacific (Fig. 6b). There appears to be no clear pattern in pairwise correlations for the individual or mixed proxies (Fig. 6c). For summer SST, the clusters are still evident but are less pronounced (Fig. 6d), and again there is no clear pattern for the individual or mixed proxies and ocean basins (Fig. 6e and f).

Finally, we can also correlate the site-to-site correlation coefficients with separation distance (i.e., correlate ρ_{ij} with D_{ij}. This shows a weak decrease in site-to-site correlation with increasing separation, significant at $p < 0.05$ for annual SST ($\rho = -0.15$, $p = 0.002$) but not summer SST ($\rho = -0.09$, $p = 0.089$), consistent with the patterns in the histograms (Fig. 6a,c)

4. Discussion

4.1. Comparison with recent LIG SST syntheses

Our synthesis of revised LIG SST reconstructions yields estimates of mean regional SST anomalies in the Southern Ocean that are not significantly different from those of recent syntheses (Fig. 7 and Table S1.1). The only exception is the Turney et al. (2020b) 'LIG average' 129 to 116 ka summer SST, which is notably cooler than both ours and that of Capron et al. (2014). In this respect it is encouraging that the different approaches followed by each study have arrived at somewhat similar answers, at least for the magnitude of LIG warming. There is also common consensus that the Southern Ocean LIG optimum had very likely ended by 115 ka.

Despite the general similarities, the underlying approaches differ in some important aspects which can be important, for example when comparing these results with climate simulations. Therefore, we discuss here what these different estimates, particularly the uncertainties, represent. First, we stress that the mean and uncertainties quoted here for this study and the other syntheses have been calculated using the mean and standard deviation of SST anomalies at contributing sites south of 40°S (here reported as the mean $\pm\, t\sigma/\sqrt{n}$): they are not the uncertainties reported by the original authors. We have used these alternative estimates to enable a more consistent comparison across all studies. As noted in Section 2.6, uncertainties originally reported by Capron et al. (2014) and Hoffman et al. (2017) are in the *mean SST anomaly only at their specific sites* (the error goes to zero if the calibration and dating errors go to zero in their Monte-Carlo error analysis). In our approach using the standard deviation and t-distribution, we assume that errors are random and independent at each site, treat each site as a random sample from a distribution of regional anomalies, and thus estimate uncertainty in the *mean SST anomaly in the study region as a whole*. Neither measure is necessarily better than the other, but the difference can be important depending on how these reconstructions are used. The Monte-Carlo approach is perhaps better suited to comparisons with climate model output at a few specific sites, while our method is better suited to comparison with a regional average. However, the Monte-Carlo error analysis requires that errors are well constrained in each step of the reconstruction, and this is not the case for Southern Ocean SST reconstructions at glacial-interglacial time scales (Part 1). Furthermore, some planktic organisms may be advected many hundreds of km in the Southern Ocean, and the anomaly recorded at a core site could reflect SST changes over a wide area some distance away. This footprint may have varied with time. Therefore, for most proxies (except perhaps for foraminifera assemblages and Mg/Ca, associated with the fastest sinking group), we would question the validity of site-by-site comparisons with climate model output. Instead, the regional average anomaly could provide a more meaningful comparison with simulations.

Capron et al. (2014) and Hoffman et al. (2017) both used revised

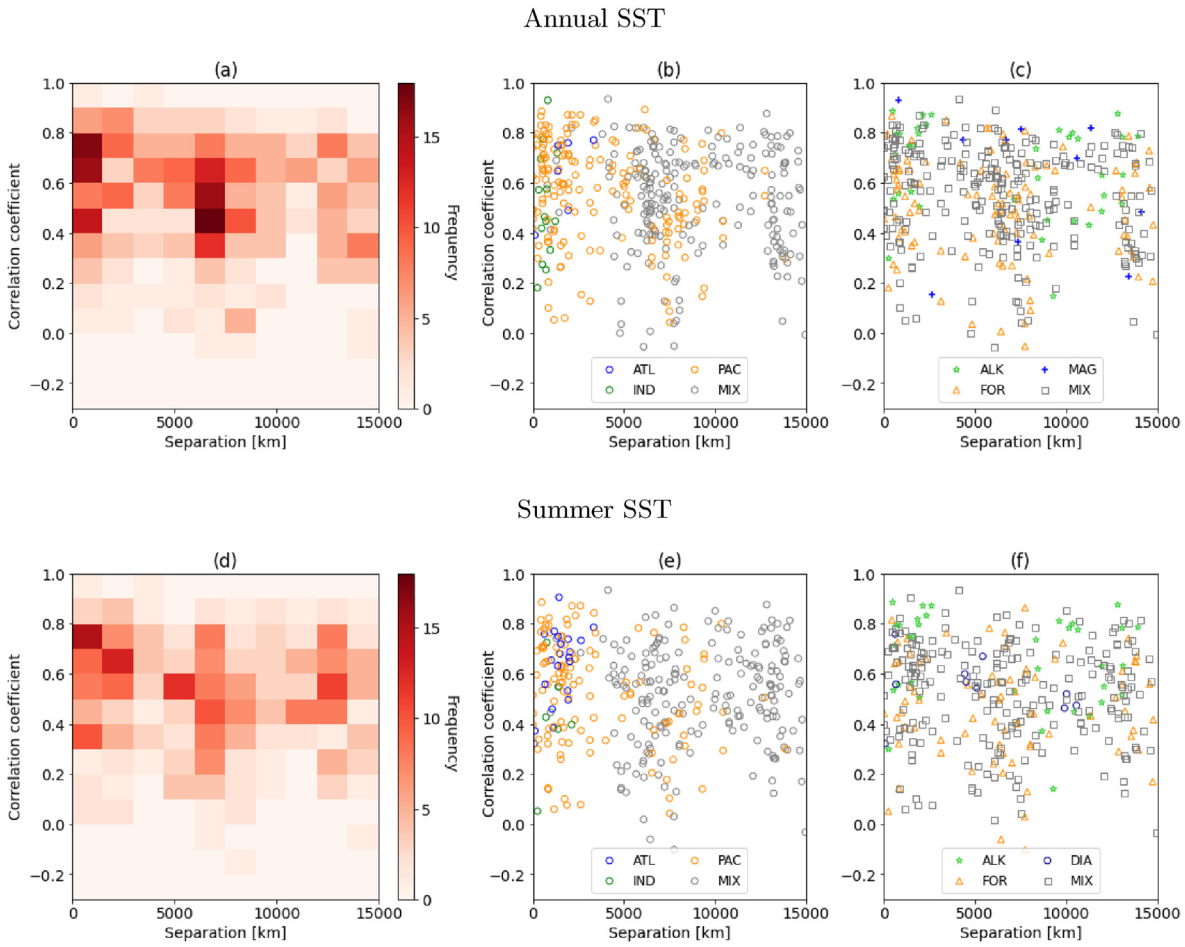

Fig. 6. For each pair of sites *i*, *j*, the separation distance (D_{ij}) and Spearman's correlation in their SST (ρ_{ij}) were calculated as described in Section 3.3. (a) The 2D histogram of pairwise separations and correlation coefficients for annual SST shows two clear clusters of site pairs: one centred on sites at close proximity ($D_{ij} < 2000$ km) with relatively strong correlation ($0.4 < \rho_{ij} < 0.8$), and a second at sites separated by ~7000 km with slightly weaker correlation ($0.4 < \rho_{ij} < 0.7$). Parts (b) and (c) show the individual points, coloured by their mutual ocean basin or proxy, respectively. Site pairs in different basins or with different proxies are coloured in grey. A broadly similar pattern is seen in respective plots for summer SST (d–f), but the clusters are weaker.

age models, consistent chronologies, and mostly the original temperature reconstructions. The only exceptions were alkenones and Mg/Ca SSTs recalculated by Hoffman et al. (2017) using the Müller et al. (1998) and Anand et al. (2003) calibrations. We have included additional sites in our study, while also excluding particular sites and proxies which we believe are less reliable. This required excluding some of the sites and proxies used in previous syntheses, most notably the radiolarian assemblages. Overall, we believe our estimate of regional mean SST should now be less susceptible to reconstruction errors associated with the individual proxies. This is supported by the relatively small RMSD and bias between the few available pairs of SSTs reconstructed from the same core (Fig. 5), compared to the RMSD and bias in the original SSTs at those sites. The much smaller difference between the foraminifera assemblage SST and the combined geochemical (alkenone Mg/Ca) SST in the revised synthesis, when compared with the original temperatures (Fig. 4), provides further validation of our approach.

Our estimated uncertainty for the Southern Ocean summer SST anomaly is very similar in magnitude to the corresponding estimate of uncertainty at Southern Ocean sites included by Capron et al. (2014), despite our apparently smaller reconstruction errors and larger number of sites (Fig. 7). Since our revised synthesis should have reduced the error associated with the temperature proxies, we must have added variance elsewhere. Time scale should not be a factor because Capron et al. (2014) used 2 kyr-wide time slices, similar to our study. The most likely source of added variance is in the age models. In our synthesis, age models have been transferred to a consistent chronology (LS16: Section 2.3), but are independent of SST as they are based on foraminiferal $\delta^{18}O$. In contrast, Capron et al. (2014) established age models by aligning the reconstructed SST anomalies directly with the Antarctic EDC reconstructed air temperature, so it is inevitable that this aspect of their approach will yield a smaller variance, as the timing of peak warming is perfectly matched across all their Southern Ocean records. In contrast, our independent alignment by $\delta^{18}O$ leads to SST peaks offset by several thousands of years between records. Therefore, while our efforts have not reduced the uncertainty in comparison to Capron et al. (2014), we believe our uncertainty now better reflects geographic variability by having a smaller contribution from SST reconstruction errors, and has not been artificially reduced by aligning SST records by temperature.

A similar comparison of our results with Hoffman et al. (2017) shows that the uncertainty in our Southern Ocean SST anomaly is considerably smaller than that calculated for their Southern Ocean sites, even though Hoffman et al. (2017) followed a similar method to Capron et al. (2014). This difference derives primarily from the choice of sites, and we highlight the records with the three

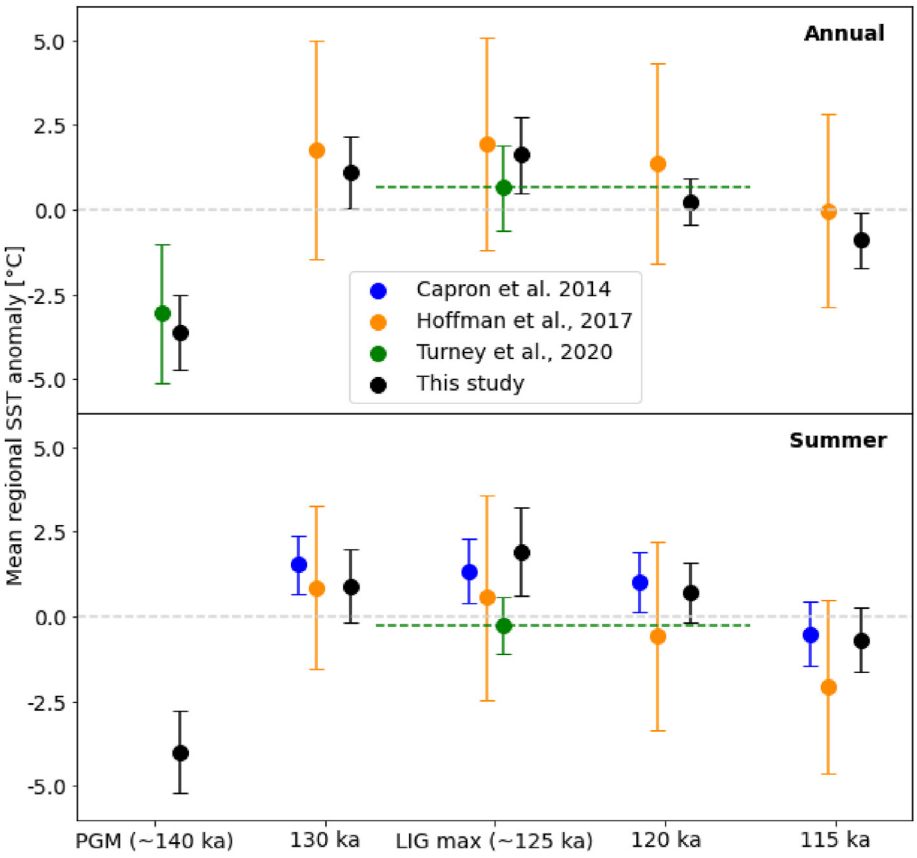

Fig. 7. Southern Ocean mean SST anomalies in this synthesis compared with those extracted from previous syntheses. Anomalies from (Capron et al., (2014) are those reported at their four time slices (130, 125, 120, 115 ka). Anomalies from Hoffman et al. (2017) are at the same times and are extracted from their 0.1 kyr resolution time series. The 'LIG' anomalies reported by Turney et al. (2020b) cover (roughly) the period 116 to 129 ka represented by the green dashed line. Note that the different studies have different southern limits and use different chronologies (See Table S1.1). The means and error bars are for sites south of 40°S, calculated using the standard deviation and t distribution: please note *these are not the original errors reported by the respective authors.* (For interpretation of the references to colour in this figure legend, the reader is referred to the Web version of this article.)

strongest annual SST anomalies at 125 ka in the Hoffman et al. (2017) synthesis: these are ODP 1089 alkenones (+9.7 °C), MD73-025 radiolarians (−7.7 °C), and MD97-2120 Mg/Ca (+7.3 °C). The ODP 1089 alkenones reconstruction was excluded from our synthesis because of reported sediment re-working (Sachs and Anderson, 2003). We excluded MD73-025 as we chose to exclude the radiolarians proxy, because of advection bias (Part 1). Finally, our reconstructed SST anomaly for MD97-2120 at 125 ka (the mean of 124 and 126 ka) was only +1.9 °C because we used a revised Mg/Ca calibration for *G. bulloides* Mg/Ca based on Southern Hemisphere mid-latitude core-tops (temperature range 2–18 °C, see Part 1), whereas Hoffman et al. (2017) used the Anand et al. (2003) multi-species Mg/Ca calibration based on sediment trap data from the Sargasso Sea (temperature range ~14–27 °C). These differences highlight the benefits of a regional synthesis and calibrations. Another potential factor is the choice of age models: although Hoffman et al. (2017) aligned their Southern Ocean basin-specific reference cores with EDC air temperature (similar to Capron et al., 2014), the remaining cores within each ocean basin were aligned to the respective reference core by benthic foraminiferal $\delta^{18}O$. This lead to differences reaching 5–10 kyr in age models at sites used by both Hoffman et al. (2017) and Capron et al. (2014). The age modelling approach of Hoffman et al. (2017) will tend to introduce more variance than that of Capron et al. (2014) because the former less strongly forces synchronous SST changes across all records than the latter.

Rather than focusing on the amplitude of SST changes, Chadwick et al. (2020) evaluated the timing of LIG SST peaks in the Southern Ocean marine sediment cores. Although the differences in timings of peaks were not statistically significant across the three main basins, evaluating timing is a challenging task: dating uncertainties of commonly 1–4 kyr, and a limited number of records with sufficient resolution (6–14 in each basin), are further compounded with uncertainties in identifying peaks in temperature records with low signal to noise ratio. We would face the same problems here, and therefore do not discuss regional differences in the timing of peak warmth.

4.2. Penultimate glacial maximum (PGM) SST anomalies

The PGM has seen less interest than the LIG in past studies, and relevant temperature syntheses are correspondingly fewer. Neither Capron et al. (2014) nor Hoffman et al. (2017) provided SST estimates earlier than 130 ka. However, Turney et al. (2020b) included annual temperature estimates for 140 to 135 ka, which closely match our 142 ka PGM estimate (Fig. 2). The greater uncertainty in the Turney et al. (2020b) pre-LIG SST, despite their greater number of sites, most likely reflects their inclusion of more proxy types and use of the original reconstructions.

Our reconstructed PGM temperature anomalies are similar to those of the LGM (Fig. 2 and Table 1), and also the MIS 4 stadial (71–59 ka). Although we do not focus on MIS 4, and do not include

all the available records for that period, the comparison is nevertheless interesting given other recently reported evidence for full glacial conditions during MIS 4 in the Southern Hemisphere (De Deckker et al., 2019). However, in contrast to the last glacial where temperatures likely followed a gradual cooling trend over the ~40 kyr prior to the LGM, our reconstruction indicates (with low confidence) a flatter long-term trend through the penultimate glacial. Although there is some distinct variability at 10 kyr time scales, these remain within the wide uncertainties. Such high uncertainties arise partly due to the relatively low number of records through that period, but potentially also because of uncertain dating: there are few distinct events in the stable isotopes record during the penultimate glacial (Lisiecki and Stern, 2016).

The lower interest in the PGM when compared to LIG should not indicate its lack of importance in understanding Southern Hemisphere ice sheet and climate response to LIG warming. Using the modern Antarctic Ice Sheet volume of 27 million km^3 (Fretwell et al., 2013), an ice density of 917 kg m^{-3}, and a typical accumulation rate of 100 kg m^{-2} yr^{-1} over an ice surface area of 121×10^{11} m^2 (Arthern et al., 2006), we crudely estimate the *average* residence time of ice in Antarctica as 20 kyr. Of course some ice is much older; at EDC, the period from 140 to 125 ka is represented in ice 1800 to 1600 m below the surface, compared to a total ice thickness of 3300 m at that site (Jouzel et al., 2007). Given such long time scales, both the geometry and ice temperature of the AIS at the onset of the LIG will have been influenced by climate throughout the penultimate glacial (and likely earlier). Therefore, the penultimate glacial climate is very relevant to understanding the LIG and its strength as an analogue for AIS response to future warming, whether in terms of ice-ocean-climate feedbacks or sea-level rise. Ongoing PMIP4 experiments (Menviel et al., 2019) and ice sheet modelling efforts (e.g., Albrecht et al., 2020; Clark et al., 2020) will hopefully provide a better understanding of Southern Hemisphere climate and ice sheet dynamics during this period.

4.3. Spatial variability

Evaluation of the core-top datasets and calibrations relevant to each proxy in Part 1 showed reconstruction errors of up to 2.6 °C, while SST reconstructions at cores with multiple proxies (Fig. 5) showed RMSDs up to 1.7 °C (and individual time slices with much larger differences). For comparison, the magnitude of the glacial-interglacial SST cycle was ~5 °C (Fig. 2). Given these relatively high uncertainties at a low number of individual sites, we do not discuss SST anomalies in smaller spatial subsets of records such as specific ocean basins or latitude bands. However, as described in Section 3.3, we can analyse the distribution of correlations between site pairs.

Overall, there was a weak decrease in the strength of correlation between sites separated by increasing distances (Section 3.3 and Fig. 6). Note that clustering of points along the separation axis in Fig. 6 reflects spatial clustering of the reconstructions as evident in Fig. 3. The study region 57°S to 40°S represents a circumpolar band of width 1900 km. Therefore, the weaker correlation in the clusters of sites separated by > 5000 km, compared to that in the cluster of sites separated by < 2500 km (Fig. 6a), must be attributed to decreasing correlation with increasing difference in longitude. The reason for this is evident in Fig. 6b, where the cluster of site pairs with relatively strong correlation at short separation is primarily composed of pairs in the same ocean basin (Atlantic or Pacific). Meanwhile, the cluster of site pairs with slightly weaker correlation at separations of ~7000 km is primarily composed of pairs either in different ocean basins or widely separated in the Pacific. This is interpreted as evidence for distinct regional signals superimposed on larger scale (circumpolar) changes.

The relatively high proportion of site pairs with weak correlation (e.g. $\rho < 0.4$), even when using the same proxy at sites separated by < 1000 km (Fig. 6c), suggests considerable variance in reconstructed temporal changes even at small spatial scales. Whether this is due to reconstruction errors or geographic variability is unclear, but we emphasise that such differences could strongly influence age models established using SST.

Another potentially interesting aspect of the reconstruction would be the changing strength of the meridional SST gradient through the LIG, but we do not discuss this here because the contribution of different proxy types varies with latitude. As a result, real changes cannot be confidently separated from methodological artefacts. These could include different sets of contributing sites and proxies at different latitudes, or latitude-dependent changes in the seasonal responses of different proxies.

4.4. Link between SST and AIS air temperature over two glacial cycles

Since we have not aligned our marine core SST reconstructions directly with Antarctic Ice Sheet air temperature, we can meaningfully compare changes in these two regions over the last two glacial cycles. Air temperature reconstructions from water stable isotopes in East Antarctic (EAIS) ice cores are available at Vostok (Petit et al., 1999), Dome Fuji (Watanabe et al., 2003), EPICA Dronning Maud Land (EDML)(EPICA Community Members, 2006), EDC (Jouzel et al., 2007), and Talos Dome (TALDICE) (Stenni et al., 2011). Climatic changes have been relatively homogeneous between these sites (Masson-Delmotte et al., 2011), and here we use a five-site average (Parrenin et al., 2013) resampled to 2 kyr following the method used above for the marine sediment cores. See Masson-Delmotte et al. (2011) and Parrenin et al. (2013) for further details and a discussion of error sources.

Significantly, we find that the relationship between Southern Ocean SST and EAIS surface air temperature during the penultimate glacial cycle (MIS 6 and 5; 190 to 80 ka) was very similar to that followed in the current cycle (MIS 4 to 1; 80 ka to present) (Fig. 8). The close relationship is interesting firstly because the provenance of precipitation at the ice core sites under modern conditions was considered to be the Southern Ocean between 40 and 50°S (Masson-Delmotte et al., 2011), consistent with the location of most of our SST reconstructions. Secondly, the consistency between the two glacial cycles suggests that *broad-scale* features of the Southern Hemisphere mid-to high-latitude climate were likely to have been similar at respective stages in both glacial cycles. This provides a little more confidence that ice sheet response to warmer conditions in the LIG, for which there is no modern analogue, could be representative of ice sheet response to future warming in the current glacial cycle. Note that this result only applies to time scales longer than 2 kyr.

The trajectory in Fig. 8 appears to show weak hysteresis, with relatively cooler Southern Ocean SST during deglaciation. Although this could be interpreted as being consistent with the effects of freshwater fluxes into the Southern Ocean from Antarctica (Fogwill et al., 2015; Mackie et al., 2020), the errors in the dating and in the temperature reconstructions mean this hysteresis should not be considered as a significant result.

5. Conclusions

In this two-part study we have evaluated SST proxies relevant to the Southern Ocean at glacial-interglacial time scales (Part 1: Chandler and Langebroek, 2021), and used the resulting recommendations in the present paper (Part 2) to reconstruct SST through the penultimate glacial cycle. This included the last

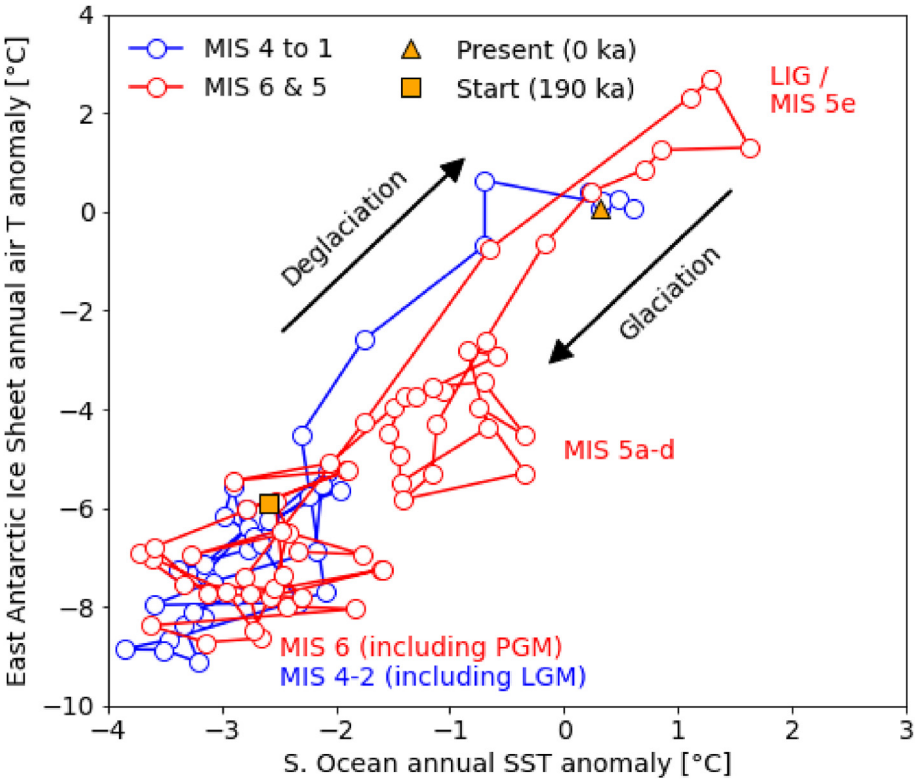

Fig. 8. Relationship between East Antarctic Ice Sheet (EAIS) surface air temperature and Southern Ocean SST over the last 2 glacial cycles (marine isotope stages 6 to 1). Starting in the penultimate glacial at 190 ka (orange square), a point is plotted every 2 kyr along a trajectory that initially lies in the cluster of red points at cold temperatures. After the PGM (142 ka), the trajectory rises along the upper red curve to the LIG optimum (126 ka), before cooling along the lower red curve to the cluster of points at intermediate temperatures (MIS 5d-a). The trajectory changes to blue at the start of MIS 4 (72 ka), and returns to cold temperatures through the last glacial. After the LGM, the upper blue curve tracks deglacial warming towards the cluster of points representing the Holocene and present (orange triangle). EAIS air temperature is resampled from Parrenin et al. (2013). Note that uncertainties in SST are typically 1–2 °C (see Fig. 2). (For interpretation of the references to colour in this figure legend, the reader is referred to the Web version of this article.)

interglacial (LIG), a period commonly used as an analogue for climate and/or ice sheet response to warming in the near future. In this second part we reach the following conclusions.

- Based on the recommended proxies and calibrations for this region and time period, we find that the LIG Southern Ocean SST anomaly peaked at 126 ka (+1.6 ± 0.9 °C annual SST; +1.9 ± 1.3 °C summer SST: Fig. 2). This is broadly consistent with other recent estimates (Fig. 7). However, our reported uncertainties better reflect geographic variability, as we have reduced errors in the individual temperature reconstructions.
- PGM cooling reached −3.6 ± 1.0 °C (annual SST) or −4.0 ± 1.2 °C (summer SST). The long-term SST trend during the penultimate glacial appears relatively flat from 186 to 142 ka.
- The reconstructed mean SST during the penultimate glacial and LIG is robust to different choices of proxies, resampling resolution, and dating method. However, our revised calibrations reduce the variance amongst different proxies (Fig. 4).
- Due to potentially large and poorly-constrained errors in individual reconstructions (e.g., advection, seasonality, depth, calibrations: see Part 1 and Fig. 5), we do not recommend detailed interpretations or comparisons of temperature records from small numbers of sites. Instead, comparisons with model simulations should focus on the Southern Ocean regional mean, treating the individual sites as random samples from this region.
- Weakly decreasing correlation between annual SST time series at site pairs separated by increasing distance was interpreted as evidence for distinct regional signals superimposed on larger scale (circumpolar) changes (Fig. 6). A high proportion of site pairs with weak correlation, even when using the same proxy at sites separated by < 1000 km (Fig. 6c), suggests considerable variance in reconstructed temporal changes even at small spatial scales. This could strongly influence age models established using SST.
- Southern Ocean (40–57°S) and Antarctic surface air temperatures have been confined to a narrow trajectory over the last two glacial cycles (Fig. 8). This close relationship provides increased confidence that broad-scale climatic features of the penultimate glacial cycle are relevant as analogues for near-future climate warming.

Despite our efforts and those of previous similar studies, there is still considerable uncertainty in Southern Ocean SST reconstructions over the LIG and penultimate glacial. In particular, the representative seasonality and depth of the individual proxies, and the effects of lateral advection, both need to be better quantified in the Southern Ocean. The geographic coverage is also sparse in this region, particularly south of ~ 50°S. While not helping the low spatial coverage, additional SST proxy records from existing sites which currently have one SST reconstruction will be very valuable in helping to empirically assess the strengths and weaknesses of each proxy under past climates. Currently, we can only really evaluate proxies under modern conditions in the Southern Ocean, as there are too few sites with multiple temperature reconstructions from one core.

Declaration of competing interest

The authors declare that they have no known competing financial interests or personal relationships that could have appeared to influence the work reported in this paper.

Acknowledgements

This study was funded by the European Union's Horizon 2020 research and innovation programme under grant agreement no. 820575 (TiPACCs). We gratefully acknowledge the many authors of the original temperature reconstructions and core-top sediment datasets, who have made their data available for use in this study. We acknowledge the developers of the open-source software used for data analysis and presentation (WebPlotDigitiser and several Python packages). Finally, we thank two anonymous reviewers for their helpful suggestions.

Data availability

Data for most original SST reconstructions and for the calibrations are already available from the Pangaea (https://www.pangaea.de) or NOAA (https://www.ncdc.noaa.gov/data-access/paleoclimatology-data) archives. Our revised SST records at 2 kyr resolution, and corresponding summary statistics, are also available from Pangaea (dataset in review).

Author contributions

DC carried out the data analysis. Both authors contributed to writing the paper.

Appendix. Marine sediment core locations and data sources

Table A1
Marine sediment core locations and data sources for sites selected in the revised synthesis. Mg/Ca data are all for *G. bulloides*. *SST used as in original publication (not recalculated). †Digitised from original publication.

Site	Location & water depth	Stable oxygen isotopes for age model	SST Source data
CHAT-1K	41.2S, −171.5E 3665 m	Benthic δ^{18}O (*Uvigerina* spp.): Weaver et al. (1998)	FOR: Weaver et al. (1998)
DSDP-593	40.5S, 167.7E 1050 m	Benthic δ^{18}O (*Uvigerina* spp.): Dudley and Nelson (1994)	ALK: McClymont et al. (2016)
DSDP-594	45.5S, 174.9E 1204 m	Benthic δ^{18}O (*Uvigerina* spp.): Dudley and Nelson (1994)	FOR: Schaefer et al. (2005)
E45-29	44.9S, 106.5E 3867 m	Planktic δ^{18}O (*G. bulloides*): Howard and Prell (1992)	FOR: Howard and Prell (1992)
E49-17	48.3S, 90.2E 3546 m	Planktic δ^{18}O (*G. bulloides*): Howard and Prell (1992)	FOR: Howard and Prell (1992)
E49-18	46.1S, 90.2E 3282 m	Planktic δ^{18}O (*G. bulloides*): Howard and Prell (1992)	FOR: Howard and Prell (1992) Mg/Ca: Rickaby and Elderfield (1999)
E49-19	43.9S, 90.1E 3057 m	Planktic δ^{18}O (*G. bulloides*): Rickaby and Elderfield (1999)	Mg/Ca: Rickaby and Elderfield (1999)
E49-21	42.2S, 94.9E 3319 m	Planktic δ^{18}O (*G. bulloides*): Howard and Prell (1992)	FOR: Howard and Prell (1992)
FR1/94-GC3	44.3S, 150.0E 2667 m	Benthic δ^{18}O (*C.wuellerstorfi*): De Deckker et al. (2019)	ALK: Pelejero et al. (2006) FOR: De Deckker et al. (2019)
GeoB3327-5	43.2S, −80.0E 3531 m	Benthic δ^{18}O (*Cibicides* spp.): Ho et al. (2012)	ALK: Ho et al. (2012)
KH94-4	48.1S 146.9E 2283 m	Planktic δ^{18}O (*G. bulloides*): Ikehara et al. (1997)	ALK†: Ikehara et al. (1997).
MD02-2488	46.5S, 88.0E 3420 m	Benthic δ^{18}O (*C. kullenbergi*): Govin et al. (2009)	FOR: Govin et al. (2009).
MD02-2588	41.2, 25.5E 2907 m	Benthic δ^{18}O (*C. wuellerstorfi*): Starr et al. (2020)	ALK: Romero et al. (2015)
MD06-2986	43.4S, 167.9E 1477 m	Benthic δ^{18}O (*C. wuellerstorfi*): Ronge et al. (2015)	FOR: Hayward et al. (2012)
MD84-551	55.0S, 73.3E 2230 m	Planktic δ^{18}O (*N. pachyderma*): Pichon et al. (1992)	DIA†*: Pichon et al. (1992).
MD88-770	46.0S, 96.5E 3290 m	Benthic δ^{18}O (mixed spp.): Sowers et al. (1993)	FOR*: Barrows et al. (2007)
MD97-2106	45.2S, 146.3E 3310 m	Benthic δ^{18}O (sp.?): Moy et al. (2006)	None: used only to compare benthic and planktic δ^{18}O.
MD97-2120	45.5S, 174.6E 1210 m	Planktic δ^{18}O (sp.?): Pahnke et al. (2003)	ALK: Pahnke and Sachs (2006) Mg/Ca: Pahnke et al. (2003)
MD97-2121	40.4S, 178.0E 3014 m	Benthic δ^{18}O (sp.?): Pahnke and Sachs (2006)	ALK: Pahnke and Sachs (2006)
ODP177 1090	42.9S, 8.9E 3702 m	Benthic δ^{18}O (*C. wuellerstorfi*): Venz and Hodell (2002)	ALK: Martínez-Garcia et al. (2009)
ODP177 1094	53.2S, 5.1E 2807 m	Benthic δ^{18}O (*Cibicidoides* spp., *Melonis pompilioides*): Hasenfratz et al. (2019)	DIA*: Bianchi and Gersonde (2002)
ODP181 1123	41.8S, −171.5E 3290 m	Benthic δ^{18}O (*Uvigerina* spp.): Elderfield et al. (2012)	FOR: Hayward et al. (2008)
PS1768-8	52.6S, 4.5E 3299 m	Planktic δ^{18}O (*N. pachyderma*): Niebler (1995)	DIA*: Zielinski et al. (1998)

Table A1 (*continued*)

Site	Location & water depth	Stable oxygen isotopes for age model	SST Source data
PS2102-2	53.1S, −5.0E 3299 m	Planktic δ^{18}O (*N. pachyderma*): Bianchi and Gersonde (2002)	DIA†*: Bianchi and Gersonde (2002).
PS2489-2	42.9S, 9.0E 3794 m	Benthic δ^{18}O (Mixed spp.): Becquey and Gersonde (2003)	FOR: Becquey and Gersonde (2003).
PS2495-3	41.3S, −14.5E 3134 m	Benthic δ^{18}O (*Cibicidoides* spp.): Mackensen et al. (2001)	FOR: Niebler (2004)
PS75/059-2	54.2S, −125.4E 3613 m	Planktic δ^{18}O (*G. bulloides*): Tapia et al. (2019)	Mg/Ca: Tapia et al. (2019)
R657	42.4S, 178.5E 1408 m	Benthic δ^{18}O (*Uvigerina* spp.): Weaver et al. (1998)	FOR: Weaver et al. (1998)
RC11-120	43.5S, 79.9E 3135 m	Planktic δ^{18}O (*G. bulloides*): Mashiotta et al. (1999)	Mg/Ca: Mashiotta et al. (1999)
SO136-111	56.7S, 160.2E 3900 m	Planktic δ^{18}O (*N. pachyderma*): Crosta et al. (2004)	DIA*: Crosta et al. (2004)
SO136-GC3	42.3S, 169.9E 958 m	Planktic δ^{18}O (*G. bulloides*): Barrows et al. (2007)	ALK: Pelejero et al. (2006) FOR*: Barrows et al. (2007)

Appendix B. Supplementary data

Supplementary data to this article can be found online at https://doi.org/10.1016/j.quascirev.2021.107190.

References

Albrecht, T., Winkelmann, R., Levermann, A., 2020. Glacial-cycle simulations of the antarctic ice sheet with the parallel ice sheet model (PISM) – Part 1: boundary conditions and climatic forcing. Cryosphere 14 (2), 599–632.

Anand, P., Elderfield, H., Conte, M.H., 2003. Calibration of Mg/Ca thermometry in planktonic foraminifera from a sediment trap time series. Paleoceanography 18 (2).

Arthern, R.J., Winebrenner, D.P., Vaughan, D.G., 2006. Antarctic snow accumulation mapped using polarization of 4.3-cm wavelength microwave emission. J. Geophys. Res. Atmos. 111 (D6).

Barrows, T.T., Juggins, S., 2005. Sea-surface temperatures around the Australian margin and Indian ocean during the last glacial maximum. Quat. Sci. Rev. 24 (7), 1017–1047.

Barrows, T.T., Juggins, S., De Deckker, P., Calvo, E., Pelejero, C., 2007. Long-term sea surface temperature and climate change in the Australian–New Zealand region. Paleoceanography 22 (2).

Batchelder, H.P., 2006. Forward-in-Time-/Backward-in-Time-Trajectory (FITT/BITT) modeling of particles and organisms in the coastal ocean. J. Atmos. Ocean. Technol. 23 (5), 727–741.

Bazin, L., Landais, A., Lemieux-Dudon, B., Toyé Mahamadou Kele, H., Veres, D., Parrenin, F., Martinerie, P., Ritz, C., Capron, E., Lipenkov, V., Loutre, M.-F., Raynaud, D., Vinther, B., Svensson, A., Rasmussen, S.O., Severi, M., Blunier, T., Leuenberger, M., Fischer, H., Masson-Delmotte, V., Chappellaz, J., Wolff, E., 2013. An optimized multi-proxy, multi-site Antarctic ice and gas orbital chronology (AICC2012): 120–800 ka. Clim. Past 9 (4), 1715–1731.

Becquey, S., Gersonde, R., 2003. A 0.55-Ma paleotemperature record from the subantarctic zone: implications for antarctic circumpolar current development. Paleoceanography 18 (1), 1014.

Bianchi, C., Gersonde, R., 2002. The Southern Ocean surface between marine isotope stages 6 and 5d: shape and timing of climate changes. Palaeogeogr. Palaeoclimatol. Palaeoecol. 187 (1), 151–177.

Bintanja, R., van Oldenborgh, G.J., Katsman, C.A., 2015. The effect of increased fresh water from Antarctic ice shelves on future trends in Antarctic sea ice. Ann. Glaciol. 56 (69), 120–126.

Capron, E., Govin, A., Stone, E.J., Masson-Delmotte, V., Mulitza, S., Otto-Bliesner, B., Rasmussen, T.L., Sime, L.C., Waelbroeck, C., Wolff, E.W., 2014. Temporal and spatial structure of multi-millennial temperature changes at high latitudes during the Last Interglacial. Quat. Sci. Rev. 103, 116–133.

Chadwick, M., Allen, C.S., Sime, L.C., Hillenbrand, C.-D., 2020. Analysing the timing of peak warming and minimum winter sea-ice extent in the Southern Ocean during MIS 5e. Quat. Sci. Rev. 229, 106134.

Chandler, D., Langebroek, P., 2021. Southern Ocean sea surface temperature synthesis: Part 1. Penultimate glacial and last interglacial. Q. Sci. Rev. 271, 107191.

Clark, P.U., He, F., Golledge, N.R., Mitrovica, J.X., Dutton, A., Hoffman, J.S., Dendy, S., 2020. Oceanic forcing of penultimate deglacial and last interglacial sea-level rise. Nature 577 (7792), 660–664.

Crosta, X., Sturm, A., Armand, L., Pichon, J.-J., 2004. Late Quaternary sea ice history in the Indian sector of the Southern Ocean as recorded by diatom assemblages. Mar. Micropaleontol. 50 (3), 209–223.

De Deckker, P., Barrows, T.T., Stuut, J.-B.W., van der Kaars, S., Ayress, M.A., Rogers, J., Chaproniere, G., 2019. Land–sea correlations in the Australian region: 460ka of changes recorded in a deep-sea core offshore Tasmania. Part 2: the marine compared with the terrestrial record. Aust. J. Earth Sci. 66 (1), 17–36.

DeConto, R.M., Pollard, D., Alley, R.B., Velicogna, I., Gasson, E., Gomez, N., Sadai, S., Condron, A., Gilford, D.M., Ashe, E.L., Kopp, R.E., Li, D., Dutton, A., 2021. The Paris Climate Agreement and future sea-level rise from Antarctica. Nature 593 (7857), 83–89.

Dudley, W.C., Nelson, C.S., 1994. The influence of non-equilibrium isotope fractionation on the Quaternary calcareous nannofossil stable isotope signal in the southwest Pacific Ocean, DSDP Site 594. Mar. Micropaleontol. 24 (1), 3–27.

Dutton, A., Carlson, A.E., Long, A.J., Milne, G.A., Clark, P.U., DeConto, R., Horton, B.P., Rahmstorf, S., Raymo, M.E., 2015. Sea-level rise due to polar ice-sheet mass loss during past warm periods. Science 349 (6244), aaa4019.

Elderfield, H., Ferretti, P., Greaves, M., Crowhurst, S., McCave, I.N., Hodell, D., Piotrowski, A.M., 2012. Evolution of ocean temperature and ice volume through the mid-pleistocene climate transition. Science 337 (6095), 704–709.

EPICA Community Members, Barbante, C., Barnola, J.-M., Becagli, S., Beer, J., Bigler, M., Boutron, C., Blunier, T., Castellano, E., Cattani, O., Chappellaz, J., Dahl-Jensen, D., Debret, M., Delmonte, B., Dick, D., Falourd, S., Faria, S., Federer, U., Fischer, H., Freitag, J., Frenzel, A., Fritzsche, D., Fundel, F., Gabrielli, P., Gaspari, V., Gersonde, R., Graf, W., Grigoriev, D., Hamann, I., Hansson, M., Hoffmann, G., Hutterli, M.A., Huybrechts, P., Isaksson, E., Johnsen, S., Jouzel, J., Kaczmarska, M., Karlin, T., Kaufmann, P., Kipfstuhl, S., Kohno, M., Lambert, F., Lambrecht, A., Lambrecht, A., Landais, A., Lawer, G., Leuenberger, M., Littot, G., Loulergue, L., Lüthi, D., Maggi, V., Marino, F., Masson-Delmotte, V., Meyer, H., Miller, H., Mulvaney, R., Narcisi, B., Oerlemans, J., Oerter, H., Parrenin, F., Petit, J.-R., Raisbeck, G., Raynaud, D., Röthlisberger, R., Ruth, U., Rybak, O., Severi, M., Schmitt, J., Schwander, J., Siegenthaler, U., Siggaard-Andersen, M.L., Spahni, R., Steffensen, J.P., Stenni, B., Stocker, T.F., Tison, J.-L., Traversi, R., Udisti, R., Valero-Delgado, F., van den Broeke, M.R., van de Wal, R.S.W., Wagenbach, D., Wegner, A., Weiler, K., Wilhelms, F., Winther, J.-G., Wolff, E., 2006. One-to-one coupling of glacial climate variability in Greenland and Antarctica. Nature 444 (7116), 195–198.

Fogwill, C.J., Phipps, S.J., Turney, C.S.M., Golledge, N.R., 2015. Sensitivity of the Southern Ocean to enhanced regional Antarctic ice sheet meltwater input. Earth's Future 3 (10), 317–329.

Fretwell, P., Pritchard, H.D., Vaughan, D.G., Bamber, J.L., Barrand, N.E., Bell, R., Bianchi, C., Bingham, R.G., Blankenship, D.D., Casassa, G., Catania, G., Callens, D., Conway, H., Cook, A.J., Corr, H.F.J., Damaske, D., Damm, V., Ferraccioli, F., Forsberg, R., Fujita, S., Gim, Y., Gogineni, P., Griggs, J.A., Hindmarsh, R.C.A., Holmlund, P., Holt, J.W., Jacobel, R.W., Jenkins, A., Jokat, W., Jordan, T., King, E.C., Kohler, J., Krabill, W., Riger-Kusk, M., Langley, K.A., Leitchenkov, G., Leuschen, C., Luyendyk, B.P., Matsuoka, K., Mouginot, J., Nitsche, F.O., Nogi, Y., Nost, O.A., Popov, S.V., Rignot, E., Rippin, D.M., Rivera, A., Roberts, J., Ross, N., Siegert, M.J., Smith, A.M., Steinhage, D., Studinger, M., Sun, B., Tinto, B.K., Welch, B.C., Wilson, D., Young, D.A., Xiangbin, C., Zirizzotti, A., 2013. Bedmap2: improved ice bed, surface and thickness datasets for Antarctica. Cryosphere 7 (1), 375–393.

Gersonde, R., Abelmann, A., Brathauer, U., Becquey, S., Bianchi, C., Cortese, G., Grobe, H., Kuhn, G., Niebler, H.-S., Segl, M., Sieger, R., Zielinski, U., Fütterer, D.K., 2003. Last glacial sea surface temperatures and sea-ice extent in the Southern Ocean (Atlantic-Indian sector): a multiproxy approach. Paleoceanography 18 (3).

Gilford, D.M., Ashe, E.L., DeConto, R.M., Kopp, R.E., Pollard, D., Rovere, A., 2020. Could the last interglacial constrain projections of future antarctic ice mass loss and sea-level rise? J. Geophys. Res. Earth Surf. 125 (10), e2019JF005418.

Goelzer, H., Huybrechts, P., Loutre, M.-F., Fichefet, T., 2016. Last Interglacial climate and sea-level evolution from a coupled ice sheet–climate model. Clim. Past 12 (12), 2195–2213.

Govin, A., Michel, E., Labeyrie, L., Waelbroeck, C., Dewilde, F., Jansen, E., 2009. Evidence for northward expansion of Antarctic Bottom Water mass in the Southern Ocean during the last glacial inception. Paleoceanography 24 (1).

Guiot, J., de Vernal, A., 2011a. Is spatial autocorrelation introducing biases in the apparent accuracy of paleoclimatic reconstructions? Quat. Sci. Rev. 30 (15), 1965–1972.

Guiot, J., de Vernal, A., 2011b. QSR Correspondence "Is spatial autocorrelation introducing biases in the apparent accuracy of palaeoclimatic reconstructions?" Reply to Telford and Birks. Quat. Sci. Rev. 30 (21), 3214–3216.
Haddam, N.A., Michel, E., Siani, G., Cortese, G., Bostock, H.C., Duprat, J.M., Isguder, G., 2016. Improving past sea surface temperature reconstructions from the Southern Hemisphere oceans using planktonic foraminiferal census data. Paleoceanography 31 (6), 822–837.
Hasenfratz, A.P., Jaccard, S.L., Martínez-García, A., Sigman, D.M., Hodell, D.A., Vance, D., Bernasconi, S.M., Kleiven, H.K.F., Haumann, F.A., Haug, G.H., 2019. The residence time of Southern Ocean surface waters and the 100,000-year ice age cycle. Science 363 (6431), 1080–1084.
Hayward, B.W., Sabaa, A.T., Kolodziej, A., Crundwell, M.P., Steph, S., Scott, G.H., Neil, H.L., Bostock, H.C., Carter, L., Grenfell, H.R., 2012. Planktic foraminifera-based sea-surface temperature record in the Tasman Sea and history of the Subtropical Front around New Zealand, over the last one million years. Mar. Micropaleontol. 82–83, 13–27.
Hayward, B.W., Scott, G.H., Crundwell, M.P., Kennett, J.P., Carter, L., Neil, H.L., Sabaa, A.T., Wilson, K., Rodger, J.S., Schaefer, G., Grenfell, H.R., Li, Q., 2008. The effect of submerged plateaux on Pleistocene gyral circulation and sea-surface temperatures in the Southwest Pacific. Global Planet. Change 63 (4), 309–316.
Hernández, A., Martin-Puertas, C., Moffa-Sánchez, P., Moreno-Chamarro, E., Ortega, P., Blockley, S., Cobb, K.M., Comas-Bru, L., Giralt, S., Goosse, H., Luterbacher, J., Martrat, B., Muscheler, R., Parnell, A., Pla-Rabes, S., Sjolte, J., Scaife, A.A., Swingedouw, D., Wise, E., Xu, G., 2020. Modes of climate variability: synthesis and review of proxy-based reconstructions through the Holocene. Earth Sci. Rev. 209, 103286.
Ho, S.L., Mollenhauer, G., Lamy, F., Martínez-Garcia, A., Mohtadi, M., Gersonde, R., Hebbeln, D., Nunez-Ricardo, S., Rosell-Melé, A., Tiedemann, R., 2012. Sea surface temperature variability in the Pacific sector of the Southern Ocean over the past 700 kyr. Paleoceanography 27 (4), PA4202.
Hoffman, J.S., Clark, P.U., Parnell, A.C., He, F., 2017. Regional and global sea-surface temperatures during the last interglaciation. Science 355 (6322), 276–279.
Holden, P.B., Edwards, N.R., Wolff, E.W., Lang, N.J., Singarayer, J.S., Valdes, P.J., Stocker, T.F., 2010. Interhemispheric coupling, the West antarctic ice sheet and warm antarctic interglacials. Clim. Past 6 (4), 431–443.
Howard, W.R., Prell, W.L., 1992. Late quaternary surface circulation of the southern Indian ocean and its relationship to orbital variations. Paleoceanography 7 (1), 79–117.
Ikehara, M., Kawamura, K., Ohkouchi, N., Kimoto, K., Murayama, M., Nakamura, T., Oba, T., Taira, A., 1997. Alkenone sea surface temperature in the Southern Ocean for the last two deglaciations. Geophys. Res. Lett. 24 (6), 679–682.
Imbrie, J., Hays, J.D., Martinson, D.G., McIntyre, A., Mix, A.C., Morley, J.J., Pisias, N.G., Prell, W.L., Shackleton, N.J., 1984. The orbital theory of Pleistocene climate: support from a revised chronology of the marine d18O record. In: Berger, A., et al. (Eds.), Milankovitch and Climate. D. Riedel, Dordrecht, pp. 269–305.
Jouzel, J., Masson-Delmotte, V., Cattani, O., Dreyfus, G., Falourd, S., Hoffmann, G., Minster, B., Nouet, J., Barnola, J.M., Chappellaz, J., Fischer, H., Gallet, J.C., Johnsen, S., Leuenberger, M., Loulergue, L., Luethi, D., Oerter, H., Parrenin, F., Raisbeck, G., Raynaud, D., Schilt, A., Schwander, J., Selmo, E., Souchez, R., Spahni, R., Stauffer, B., Steffensen, J.P., Stenni, B., Stocker, T.F., Tison, J.L., Werner, M., Wolff, E.W., 2007. Orbital and millennial antarctic climate variability over the past 800,000 years. Science 317 (5839), 793–796.
Kopp, R.E., Simons, F.J., Mitrovica, J.X., Maloof, A.C., Oppenheimer, M., 2009. Probabilistic assessment of sea level during the last interglacial stage. Nature 462 (7275), 863–867.
Langebroek, P.M., Nisancioglu, K.H., 2014. Simulating last interglacial climate with NorESM: role of insolation and greenhouse gases in the timing of peak warmth. Clim. Past 10 (4), 1305–1318.
Lisiecki, L.E., Raymo, M.E., 2005. A Pliocene-Pleistocene stack of 57 globally distributed benthic δ18O records. Paleoceanography 20 (1).
Lisiecki, L.E., Raymo, M.E., 2009. Diachronous benthic δ18O responses during late Pleistocene terminations. Paleoceanography 24 (3).
Lisiecki, L.E., Stern, J.V., 2016. Regional and global benthic δ18O stacks for the last glacial cycle. Paleoceanography 31 (10), 1368–1394.
Locarnini, R.A., Mishonov, A.V., Baranova, O.K., Boyer, T.P., Zweng, M.M., Garcia, H.E., Reagan, J.R., Seidov, D., Weathers, K., Paver, C.R., Smolyar, I., 2018. World ocean atlas 2018, volume 1: Temperature. In: Mishonov, A. (Ed.), NOAA Atlas NESDIS 81. NOAA.
Mackensen, A., Rudolph, M., Kuhn, G., 2001. Late Pleistocene deep-water circulation in the subantarctic eastern Atlantic. Global Planet. Change 30 (3), 197–229.
Mackie, S., Smith, I.J., Ridley, J.K., Stevens, D.P., Langhorne, P.J., 2020. Climate response to increasing antarctic iceberg and ice shelf Melt. J. Clim. 33 (20), 8917–8938.
Martínez-Garcia, A., Rosell-Melé, A., Geibert, W., Gersonde, R., Masqué, P., Gaspari, V., Barbante, C., 2009. Links between iron supply, marine productivity, sea surface temperature, and CO2 over the last 1.1 Ma. Paleoceanography 24 (1).
Martinson, D.G., Pisias, N.G., Hays, J.D., Imbrie, J., Moore, T.C., Shackleton, N.J., 1987. Age dating and the orbital theory of the ice ages: development of a high-resolution 0 to 300,000-year chronostratigraphy 1. Quat. Res. 27 (1), 1–29.
Mashiotta, T.A., Lea, D.W., Spero, H.J., 1999. Glacial–interglacial changes in Subantarctic sea surface temperature and δ18O-water using foraminiferal Mg. Earth Planet Sci. Lett. 170 (4), 417–432.
Masson-Delmotte, V., Buiron, D., Ekaykin, A., Frezzotti, M., Gallée, H., Jouzel, J., Krinner, G., Landais, A., Motoyama, H., Oerter, H., Pol, K., Pollard, D., Ritz, C., Schlosser, E., Sime, L.C., Sodemann, H., Stenni, B., Uemura, R., Vimeux, F., 2011. A comparison of the present and last interglacial periods in six Antarctic ice cores. Clim. Past 7 (2), 397–423.
McClymont, E.L., Elmore, A.C., Kender, S., Leng, M.J., Greaves, M., Elderfield, H., 2016. Pliocene-Pleistocene evolution of sea surface and intermediate water temperatures from the southwest Pacific. Paleoceanography 31 (6), 895–913.
Menviel, L., Capron, E., Govin, A., Dutton, A., Tarasov, L., Abe-Ouchi, A., Drysdale, R.N., Gibbard, P.L., Gregoire, L., He, F., Ivanovic, R.F., Kageyama, M., Kawamura, K., Landais, A., Otto-Bliesner, B.L., Oyabu, I., Tzedakis, P.C., Wolff, E., Zhang, X., 2019. The penultimate deglaciation: protocol for Paleoclimate Modelling Intercomparison Project (PMIP) phase 4 transient numerical simulations between 140 and 127ka, version 1.0. *Geosci.* Model Dev 12 (8), 3649–3685.
Mercer, J.H., 1978. West Antarctic ice sheet and CO2 greenhouse effect: a threat of disaster. Nature 271 (5643), 321–325.
Moy, A.D., Howard, W.R., Gagan, M.K., 2006. Late quaternary palaeoceanography of the circumpolar deep water from the South tasman rise. J. Quat. Sci. 21 (7), 763–777.
Müller, P.J., Kirst, G., Ruhland, G., von Storch, I., Rosell-Melé, A., 1998. Calibration of the alkenone paleotemperature index U37K′ based on core-tops from the eastern South Atlantic and the global ocean (60°N-60°S). Geochem. Cosmochim. Acta 62 (10), 1757–1772.
Niebler, H.-S., 1995. Rekonstruktionen von Palăo-Umweltparametern anhand von stabilen Isotopen und Faunen-Vergesellschaftungen planktischer Foraminiferen im Südatlantik. Rep. Polar Res. 167, 1–198.
Niebler, H.-S., 2004. Isotopes (N. Pachyderma, Dextral) of Sediment Core PS2495-3.
Nooteboom, P.D., Bijl, P.K., van Sebille, E., von der Heydt, A.S., Dijkstra, H.A., 2019. Transport bias by ocean currents in sedimentary Microplankton assemblages: implications for paleoceanographic reconstructions. Paleoceanogr. Paleoclimatol. 34 (7), 1178–1194.
Pahnke, K., Sachs, J.P., 2006. Sea surface temperatures of southern midlatitudes 0–160 kyr B.P. Paleoceanography 21 (2).
Pahnke, K., Zahn, R., Elderfield, H., Schulz, M., 2003. 340,000-Year centennial-scale marine record of southern hemisphere climatic oscillation. Science 301 (5635), 948–952.
Parrenin, F., Barnola, J.-M., Beer, J., Blunier, T., Castellano, E., Chappellaz, J., Dreyfus, G., Fischer, H., Fujita, S., Jouzel, J., Kawamura, K., Lemieux-Dudon, B., Loulergue, L., Masson-Delmotte, V., Narcisi, B., Petit, J.-R., Raisbeck, G., Raynaud, D., Ruth, U., Schwander, J., Severi, M., Spahni, R., Steffensen, J.P., Svensson, A., Udisti, R., Waelbroeck, C., Wolff, E., 2007. The EDC3 chronology for the EPICA Dome C ice core. Clim. Past 3 (3), 485–497.
Parrenin, F., Masson-Delmotte, V., Köhler, P., Raynaud, D., Paillard, D., Schwander, J., Barbante, C., Landais, A., Wegner, A., Jouzel, J., 2013. Synchronous change of atmospheric CO2 and antarctic temperature during the last deglacial warming. Science 339 (6123), 1060–1063.
Past Interglacials Working Group of PAGES, 2016. Interglacials of the last 800,000 years. Rev. Geophys. 54 (1), 162–219.
Pedro, J.B., Jochum, M., Buizert, C., He, F., Barker, S., Rasmussen, S.O., 2018. Beyond the bipolar seesaw: toward a process understanding of interhemispheric coupling. Quat. Sci. Rev. 192, 27–46.
Pelejero, C., Calvo, E., Barrows, T.T., Logan, G.A., De Deckker, P., 2006. South Tasman Sea alkenone palaeothermometry over the last four glacial/interglacial cycles. Mar. Geol. 230 (1), 73–86.
Petit, J.R., Jouzel, J., Raynaud, D., Barkov, N.I., Barnola, J.-M., Basile, I., Bender, M., Chappellaz, J., Davis, M., Delaygue, G., Delmotte, M., Kotlyakov, V.M., Legrand, M., Lipenkov, V.Y., Lorius, C., PÉpin, L., Ritz, C., Saltzman, E., Stievenard, M., 1999. Climate and atmospheric history of the past 420,000 years from the Vostok ice core, Antarctica. Nature 399 (6735), 429–436.
Pichon, J.-J., Labeyrie, L.D., Bareille, G., Labracherie, M., Duprat, J., Jouzel, J., 1992. Surface water temperature changes in the high latitudes of the southern hemisphere over the Last Glacial-Interglacial Cycle. Paleoceanography 7 (3), 289–318.
Popova, I.M., 1986. Transportation of radiolarian shells by currents (calculations based on the example of the Kuroshio). Mar. Micropaleontol. 11 (1), 197–201.
Prahl, F.G., Muehlhausen, L.A., Zahnle, D.L., 1988. Further evaluation of long-chain alkenones as indicators of paleoceanographic conditions. Geochem. Cosmochim. Acta 52 (9), 2303–2310.
Prahl, F.G., Wakeham, S.G., 1987. Calibration of unsaturation patterns in long-chain ketone compositions for palaeotemperature assessment. Nature 330 (6146), 367–369.
Rickaby, R.E.M., Elderfield, H., 1999. Planktonic foraminiferal Cd/Ca: paleonutrients or paleotemperature? Paleoceanography 14 (3), 293–303.
Rintoul, S.R., 2018. The global influence of localized dynamics in the Southern Ocean. Nature 558 (7709), 209–218.
Rohling, E.J., Hibbert, F.D., Williams, F.H., Grant, K.M., Marino, G., Foster, G.L., Hennekam, R., de Lange, G.J., Roberts, A.P., Yu, J., Webster, J.M., Yokoyama, Y., 2017. Differences between the last two glacial maxima and implications for ice-sheet, δ18O, and sea-level reconstructions. Quat. Sci. Rev. 176, 1–28.
Romero, O.E., Kim, J.-H., Bárcena, M.A., Hall, I.R., Zahn, R., Schneider, R., 2015. High-latitude forcing of diatom productivity in the southern Agulhas Plateau during the past 350kyr. Paleoceanography 30 (2), 118–132.
Ronge, T.A., Steph, S., Tiedemann, R., Prange, M., Merkel, U., Nürnberg, D., Kuhn, G., 2015. Pushing the boundaries: glacial/interglacial variability of intermediate and deep waters in the southwest Pacific over the last 350,000 years. Paleoceanography 30 (2), 23–38.
Sachs, J.P., Anderson, R.F., 2003. Fidelity of alkenone paleotemperatures in southern

Cape Basin sediment drifts. Paleoceanography 18 (4).
Saenger, C.P., Evans, M.N., 2019. Calibration and validation of environmental controls on planktic foraminifera Mg/Ca using global core-top data. Paleoceanogr. Paleoclimatol. 34 (8), 1249–1270.
Schaefer, G., Rodger, J.S., Hayward, B.W., Kennett, J.P., Sabaa, A.T., Scott, G.H., 2005. Planktic foraminiferal and sea surface temperature record during the last 1 Myr across the Subtropical Front, Southwest Pacific. Mar. Micropaleontol. 54 (3), 191–212.
Scherer, R.P., Aldahan, A., Tulaczyk, S., Possnert, G., Engelhardt, H., Kamb, B., 1998. Pleistocene collapse of the West antarctic ice sheet. Science 281 (5373), 82–85.
Shackleton, N.J., 1974. Attainment of Isotopic Equilibrium between Ocean Water and the Benthonic Foraminifera Genus Uvigerina: Isotopic Changes in the Ocean during the Last Glacial, ume 219. C.N.R.S. Colloquium, pp. 203–209.
Sikes, E.L., Volkman, J.K., 1993. Calibration of alkenone unsaturation ratios (UK'37) for paleotemperature estimation in cold polar waters. Geochem. Cosmochim. Acta 57 (8), 1883–1889.
Sowers, T., Bender, M., Labeyrie, L., Martinson, D., Jouzel, J., Raynaud, D., Pichon, J.J., Korotkevich, Y.S., 1993. A 135,000-year Vostok-Specmap Common temporal framework. Paleoceanography 8 (6), 737–766.
Starr, A., Hall, I.R., Ziegler, M., 2020. Pleistocene Benthic Stable Isotopes and and Age-Depth Model from the Agulhas Plateau Composite (APcomp).
Stenni, B., Buiron, D., Frezzotti, M., Albani, S., Barbante, C., Bard, E., Barnola, J.M., Baroni, M., Baumgartner, M., Bonazza, M., Capron, E., Castellano, E., Chappellaz, J., Delmonte, B., Falourd, S., Genoni, L., Iacumin, P., Jouzel, J., Kipfstuhl, S., Landais, A., Lemieux-Dudon, B., Maggi, V., Masson-Delmotte, V., Mazzola, C., Minster, B., Montagnat, M., Mulvaney, R., Narcisi, B., Oerter, H., Parrenin, F., Petit, J.R., Ritz, C., Scarchilli, C., Schilt, A., Schüpbach, S., Schwander, J., Selmo, E., Severi, M., Stocker, T.F., Udisti, R., 2011. Expression of the bipolar see-saw in Antarctic climate records during the last deglaciation. Nat. Geosci. 4 (1), 46–49.
Sutter, J., Gierz, P., Grosfeld, K., Thoma, M., Lohmann, G., 2016. Ocean temperature thresholds for last interglacial West Antarctic ice sheet collapse. Geophys. Res. Lett. 43 (6), 2675–2682.
Tapia, R., Nürnberg, D., Ho, S.L., Lamy, F., Ullermann, J., Gersonde, R., Tiedemann, R., 2019. Glacial differences of Southern Ocean intermediate waters in the central south pacific. Quat. Sci. Rev. 208, 105–117.
Telford, R.J., Birks, H.J.B., 2011. QSR Correspondence "Is spatial autocorrelation introducing biases in the apparent accuracy of palaeoclimatic reconstructions?". Quat. Sci. Rev. 30 (21), 3210–3213.
Tierney, J.E., Malevich, S.B., Gray, W., Vetter, L., Thirumalai, K., 2019. Bayesian calibration of the Mg/Ca paleothermometer in planktic foraminifera. Paleoceanogr. Paleoclimatol. 34 (12), 2005–2030.
Tierney, J.E., Tingley, M.P., 2014. A Bayesian, spatially-varying calibration model for the TEX86 proxy. Geochem. Cosmochim. Acta 127, 83–106.
Tierney, J.E., Tingley, M.P., 2018. BAYSPLINE: a new calibration for the alkenone paleothermometer. Paleoceanogr. Paleoclimatol. 33 (3), 281–301.
Turney, C.S.M., Fogwill, C.J., Golledge, N.R., McKay, N.P., van Sebille, E., Jones, R.T., Etheridge, D., Rubino, M., Thornton, D.P., Davies, S.M., Ramsey, C.B., Thomas, Z.A., Bird, M.I., Munksgaard, N.C., Kohno, M., Woodward, J., Winter, K., Weyrich, L.S., Rootes, C.M., Millman, H., Albert, P.G., Rivera, A., van Ommen, T., Curran, M., Moy, A., Rahmstorf, S., Kawamura, K., Hillenbrand, C.-D., Weber, M.E., Manning, C.J., Young, J., Cooper, A., 2020a. Early Last Interglacial ocean warming drove substantial ice mass loss from Antarctica. Proc. Natl. Acad. Sci. U.S.A. 117 (8), 3996–4006.
Turney, C.S.M., Jones, R.T., McKay, N.P., van Sebille, E., Thomas, Z.A., Hillenbrand, C.-D., Fogwill, C.J., 2020b. A global mean sea surface temperature dataset for the Last Interglacial (129–116ka) and contribution of thermal expansion to sea level change. Earth Syst. Sci. Data 12 (4), 3341–3356.
Urey, H.C., Lowenstam, H.A., Epstein, S., Mckinney, C.R., 1951. Measurement of paleotemperatures and temperatures of the upper Cretaceous of England, Denmark, and the southeastern United States. GSA Bulletin 62 (4), 399–416.
van Sebille, E., Scussolini, P., Durgadoo, J.V., Peeters, F.J.C., Biastoch, A., Weijer, W., Turney, C., Paris, C.B., Zahn, R., 2015. Ocean currents generate large footprints in marine palaeoclimate proxies. Nat. Commun. 6 (6521), 1–8.
Vaughan, D.G., 2008. West Antarctic Ice Sheet collapse – the fall and rise of a paradigm. Climatic Change 91 (1), 65–79.
Venz, K.A., Hodell, D.A., 2002. New evidence for changes in plio–pleistocene deep water circulation from Southern Ocean ODP leg 177 site 1090. Palaeogeogr. Palaeoclimatol. Palaeoecol. 182 (3), 197–220.
Veres, D., Bazin, L., Landais, A., Toyé Mahamadou Kele, H., Lemieux-Dudon, B., Parrenin, F., Martinerie, P., Blayo, E., Blunier, T., Capron, E., Chappellaz, J., Rasmussen, S.O., Severi, M., Svensson, A., Vinther, B., Wolff, E.W., 2013. The Antarctic ice core chronology (AICC2012): an optimized multi-parameter and multi-site dating approach for the last 120 thousand years. Clim. Past 9 (4), 1733–1748.
Waelbroeck, C., Paul, A., Kucera, M., Rosell-Melé, A., Weinelt, M., Schneider, R., Mix, A.C., Abelmann, A., Armand, L., Bard, E., Barker, S., Barrows, T.T., Benway, H., Cacho, I., Chen, M.-T., Cortijo, E., Crosta, X., de Vernal, A., Dokken, T., Duprat, J., Elderfield, H., Eynaud, F., Gersonde, R., Hayes, A., Henry, M., Hillaire-Marcel, C., Huang, C.-C., Jansen, E., Juggins, S., Kallel, N., Kiefer, T., Kienast, M., Labeyrie, L., Leclaire, H., Londeix, L., Mangin, S., Matthiessen, J., Marret, F., Meland, M., Morey, A.E., Mulitza, S., Pflaumann, U., Pisias, N.G., Radi, T., Rochon, A., Rohling, E.J., Sbaffi, L., Schäfer-Neth, C., Solignac, S., Spero, H., Tachikawa, K., Turon, J.-L., MARGO Project Members, 2009. Constraints on the magnitude and patterns of ocean cooling at the Last Glacial Maximum. Nat. Geosci. 2 (2), 127–132.
Watanabe, O., Jouzel, J., Johnsen, S., Parrenin, F., Shoji, H., Yoshida, N., 2003. Homogeneous climate variability across East Antarctica over the past three glacial cycles. Nature 422 (6931), 509–512.
Weaver, P.P.E., Carter, L., Neil, H.L., 1998. Response of surface water masses and circulation to Late Quaternary climate change east of New Zealand. Paleoceanography 13 (1), 70–83.
Welch, B.L., 1947. The generalization of 'student's' problem when several different population variances are involved. Biometrika 34 (1–2), 28–35.
Xiao, W., Frederichs, T., Gersonde, R., Kuhn, G., Esper, O., Zhang, X., 2016. Constraining the dating of late quaternary marine sediment records from the scotia sea (Southern Ocean). Quat. Geochronol. 31, 97–118.
Yin, Q., Berger, A., 2015. Interglacial analogues of the Holocene and its natural near future. Quat. Sci. Rev. 120, 28–46.
Zielinski, U., Gersonde, R., Sieger, R., Fütterer, D., 1998. Quaternary surface water temperature estimations: calibration of a diatom transfer function for the Southern Ocean. Paleoceanography 13 (4), 365–383.